Parsec scale properties of Brightest Cluster Galaxies

Elisabetta Liuzzo [1,2]

Gabriele Giovannini [1,2]   Marcello Giroletti [2]

[1] Dipartimento di Astronomia, Università di Bologna   [2] Istituto di Radioastronomia – INAF (Bologna)

General properties of BCGs

BCGs are a unique class of sources (Yen-Ting Lin et al.2004)

most luminous (~10 L_E) + **most massive** (~ $10^{12} M_{sol}$) + **extended source** (~200 kpc)

→ cD galaxy, also giant E and D galaxy (Tonry 1987)

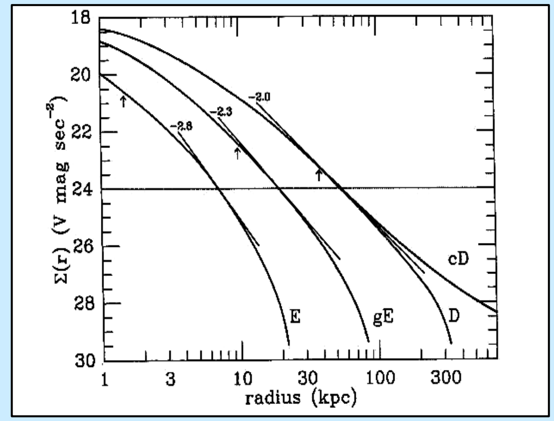

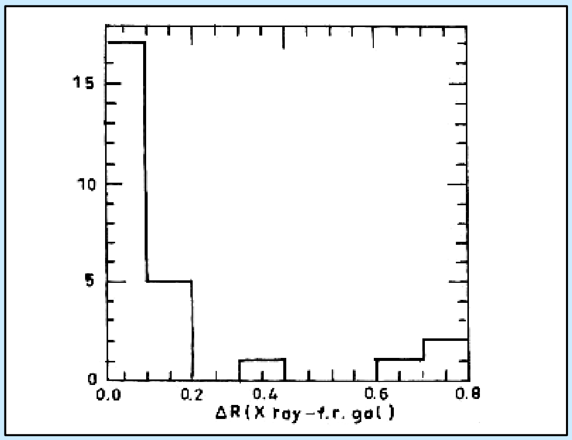

(Rhee & Latour 1991)

→ Close to the peak of the cluster X-Ray emission

Different formation history ←

-Evidence of **multiple nuclei BCGs**
(Laine et al. 2003)

(Bernardi et al. 2007)

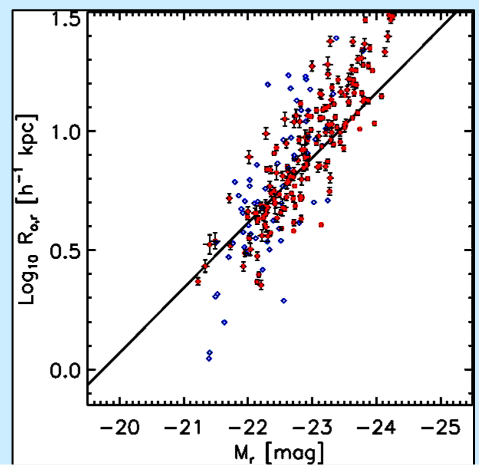

(Colors: Different BCG type)

→ In the v-space they sit near the cluster rest frame

(Oegerle & Hill 2001)

General properties of BCGs

Radio Band

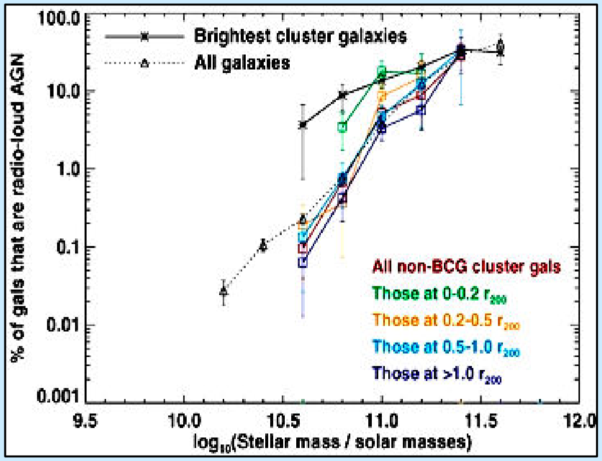

→ They are more likely to host radio-loud AGN than other galaxies of the same mass

(Best et al. 2006)

➔ different kpc scale morphologies

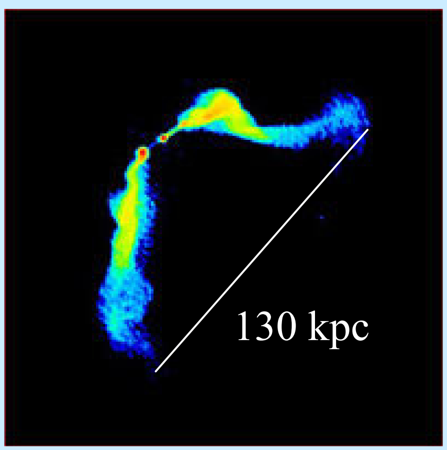

3C465 (A2634)

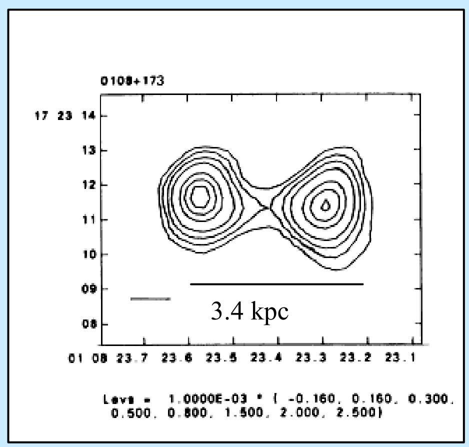

IC1634 (A154)

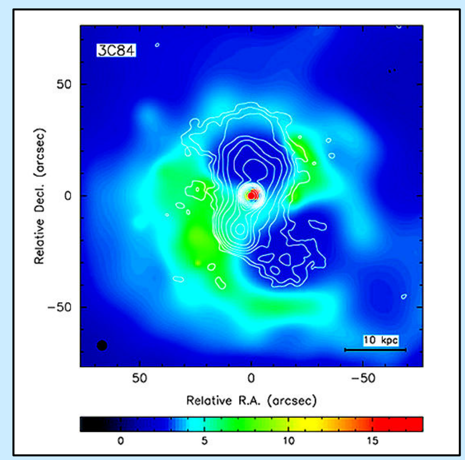

Perseus A

BCG Sample

Aim and method

(Liuzzo et al. 2010)

- The aim of the project: at mas scale, it is not yet present a **statistically study**

- Abell Clusters with DC ≤ 2 and Declination > 0^0

- no selection on cluster condition and/or BCG radio power

-23 Abell Clusters
→ total 27 objects

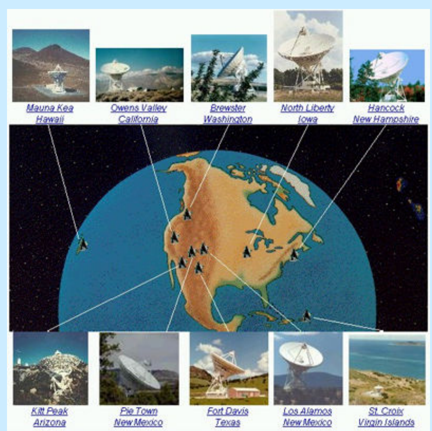

Abell Cl.	DC	z	kpc/arcsec	BCG
262	0	0.0161	0.328	NGC708
347	1	0.0187	0.380	NGC910
400	1	0.0232	0.468	3C75A
				3C75B
407	2	0.0470	0.922	UGC2489
426	0	0.0176	0.358	3C84
539	2	0.0205	0.415	UGC3274
569	1	0.0196	0.397	NGC2329
576	2	0.0381	0.755	CGCG261-059
779	1	0.0226	0.457	NGC2832
1185	2	0.0304	0.608	NGC3550
1213	2	0.0468	0.918	4C29.41
1228	1	0.0350	0.697	IC2738
1314	1	0.0341	0.679	IC708
				IC712
1367	1	0.0215	0.435	NGC3842
				3C264
1656	1	0.0232	0.468	NGC4874
2147	1	0.0356	0.708	UGC10143
2151	1	0.0371	0.737	NGC6041
				NGC6047
2152	1	0.0374	0.742	UGC10187
2162	1	0.0320	0.639	NGC6086
2197	1	0.0303	0.606	NGC6173
2199	1	0.0303	0.606	3C338
2634	1	0.0312	0.624	3C465
2666	1	0.0265	0.533	NGC7768

-5 GHz VLBA observations → news for 23 sources
(2007 June /2008 March)
- 3 hours for source in phase reference mode

- Resolution : 3mas x 1.8 mas

- Noise ~ 0.1 mJy/beam

BCG Sample

The extended sample
(Liuzzo et al. 2010)

Outside the Sample.... (to increase the statistic)

Abell Clusters but with DC>2

- **B2 0836+29II in A 690** (O'Donoghue et al. 1990; Giovannini et al. 2005);
- **Hydra A in A780** (Taylor 1996; Wise et al. 2007);
- **4C 26.42 in A1795** (Liuzzo et al. 2009a; Salomé & Combes 2004);
- **3C317 in A2052** (Venturi et al. 2004);
- **B2151+174 in A 2390** (Augusto et al. 2006);
- **PKS 2322-123 in A 2597** (Morris & Fabian 2005; Taylor et al. 1999)
- **PKS 1246-410 (NGC4696) in A 3526** (Taylor et al. 2006)

extended sample = 34 sources

At parsec scale, also nuclei of radio loud BCGs have structures sometime very complex

Results

(Liuzzo et al. 2010)

BCG	pc structure	j/cj ratio	$\beta\cos\theta$	$S_{c,5}$ mJy	$LogP_{c,5}$ W/Hz	$S_{t,408}$ mJy	$LoP_{t,408}$ W/Hz	$S_{VLBI}/S_{c,5GHz}$(%)	core dominance
NGC708	c	-	-	5	21.47	364	23.33	60	0.26
NGC910	n.d	-	2	-	-	-	-	<25	-
3C75A	1s	≥6.2	≥0.35	6	21.87	190	23.37	100	0.60
3C75B	1s	≥ 4.6	≥0.3	20	22.39	190	23.37	100	2
3C84	2s	2	0.14	28.17×10^3	25.29	51.68×10^3	25.56	80	70.79
UGC3274	n.d	-	-	<1.4	-	-	-	-	-
UGC2489	1s	≥2.8	≥0.2	4	22.32	2.83×10^3	25.17	90	0.13
NGC2329	1s	≥4.5	≥0.29	160	23.14	1300	24.05	50	4.3
CGCG261-059	1s	≥1.8	≥0.12	1.5	21.71	6.54	22.34	100	1.8
NGC2832	n.d	-	-	2.4	-	-	-	<21	-
NGC3550	n.d	-	-	<1.4	-	-	-	-	-
4C29.41	1s	≥3.8	≥0.26	41	23.33	135.2	23.84	100	8.71
IC2738	n.d	-	-	-	-	-	-	-	-
IC708	1s	≥6.5	≥0.36	110	23.47	901.1	24.39	40	5.62
IC712	n.d	-	-	14.02	22.58	48.72	23.12	<3	4.37
NGC3842	n.d	-	-	9	22.98	101.88	23.03	<8	0.36
3C264	1s	≥6	≥0.34	200	23.32	17×10^3	25.25	100	1.17
NGC4874	1s	≥1.6	≥0.09	1.1	21.13	351.96	23.63	100	0.08
UGC10143	n.d	-	-	<2	<21.77	14.87	22.64	-	<1.35
NGC6041A	c	-	-	≤0.9	≤21.92	21.5	22.84	100	1.45
NGC6047	n.d	-	-	8.3	22.42	1960	24.80	<7	0.28
UGC10187	n.d	-	-	<2	<21.81	111.7	23.56	-	<0.41
NGC6086	n.d	-	-	<1	<21.37	201.35	23.68	-	<0.12
NGC6173	1s	≥1.4	≥0.07	3.7	21.89	12.97	22.44	40	2.40
3C338	2s	2.2	0.16	480	24.01	18.12×10^3	25.59	30	3.47
3C465	1s	≥20	≥0.54	246	23.74	10.38×10^3	25.37	100	2.57
NGC7768	1s	≥1.1	≥0.02	0.74	21.08	2.6	21.62	100	1.17
B2 0836+29II	1s	≥20	≥0.54	131	24.31	1139	25.24	100	11.20
Hydra A	2s	1.2	0.04	168	24.08	132×10^3	26.98	100	0.58
4C 26.42	2s	1.4	0.07	53	23.71	3153	25.48	80	2.04
3C 317	2s	1.5	0.08	310	23.93	132×10^3	26.56	100	0.72
B2151+174	2s	4	0.27	164	25.40	538	25.92	100	53
PKS 2322-123	2s	1.2	0.04	59.3	24.0	7.2×10^3	26.11	80	1.66
PKS 1246-410	1s	≥9	0.34	64.4	22.27	2463	23.86	30	0.76

Peculiar cases of BCGs

4C 26.42 in Abell 1795 (Liuzzo et al. 2009a)

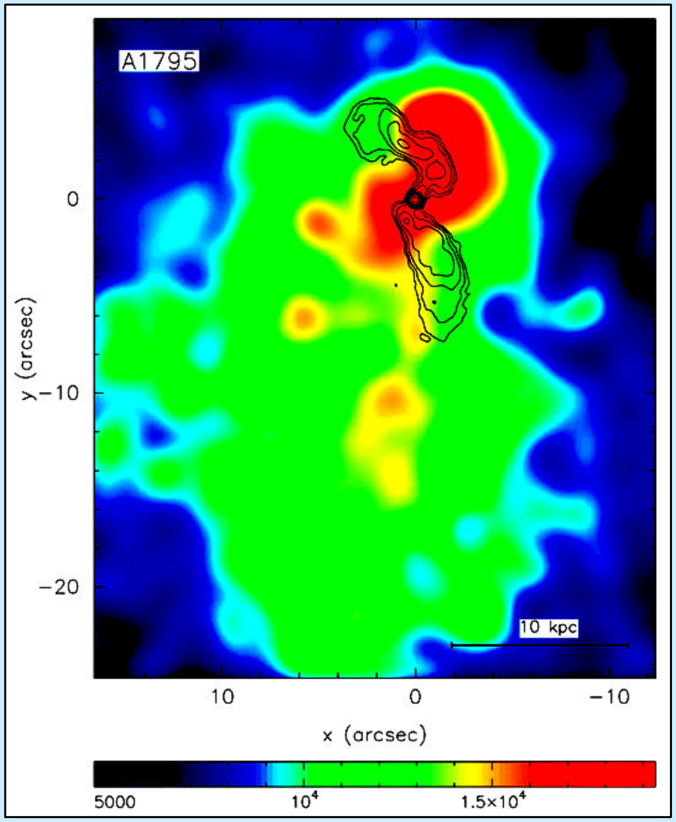

CHANDRA + VLA

General cluster and BCG information:

- $z = 0.0633$
- cool core cluster → cooling in the central 200-kpc region (Ettori et al. 2002)
- 8.5×10^{44} erg/sec in the 0.5-4.5 keV
- Mv= -23, cD galaxy
- strong emission line around cD (Capetti et al. 2000)
- molecular gas in the cD (Falcke et al. 1998)
- X-ray filament coincident with Hα (Fabian et al. 1994)
- High RM → hot (10^8 K) and dense (0.03 cm^{-3}) X-ray emitting gas (Ge et al. 1993)
- CO emission (Salomé & Combes 2003)

The central radio source:

- FRI, Z-shaped small (2 arc x 12 arcsec)
- at 408 MHz, total power LogP= 25.47 (W/Hz)
- at 5 GHz, core power LogP = 23.70 (W/Hz)

Peculiar cases of BCGs

4C 26.42 in Abell 1795

CO emission (Salomé & Combes 2003)

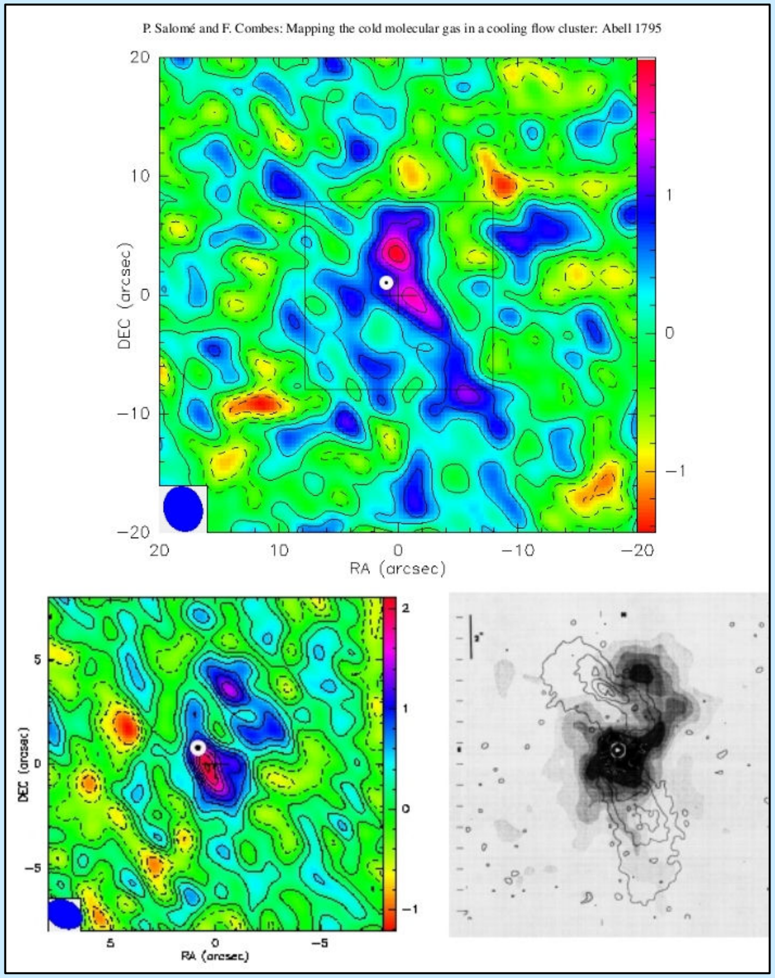

CO (1-0)

* Correlation between CO and H_α

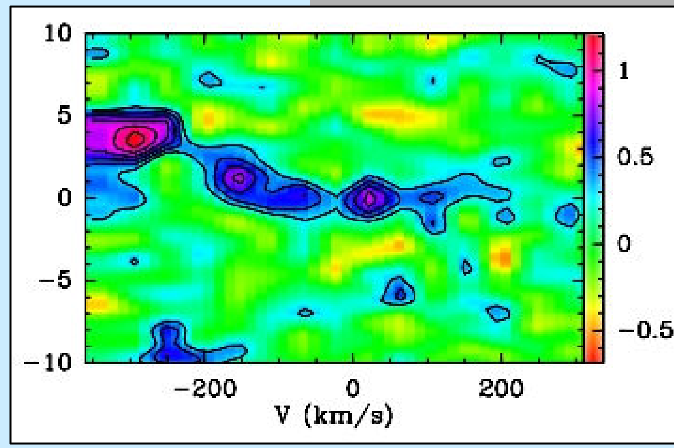

CO (1-0)

• Mass of H_2 4.8×10^9 M_{sol}

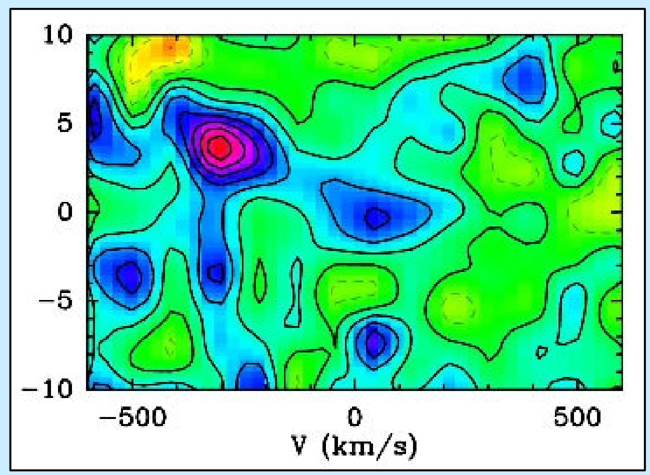

CO(2-1)

CO(2-1)

H_α + NII in grey scale and 6cm VLA (contours)

Peculiar cases of BCGs

4C 26.42 in Abell 1795 (Liuzzo et al. 2009a)

VLBA Data: → resolution (mas = 1.2 pc)

- 1.6 GHz : 2003 and 2008	11 x 6
- 5 GHz : 1997, 2005 and 2008	3.5 x 2
- 8 GHz : 2008	2 x 1
- 22 GHz : 2008	1 x 0.7

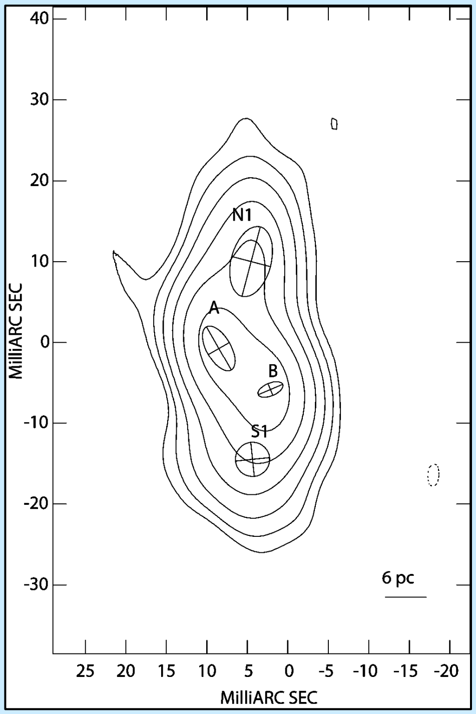

Contour levels = -0.45, 0.45, 0.9, 1.8, 3.6, 7.2, 14.4 mJy/b

Frequency GHz	Epoch yy-mm-dd	χ^2	Component	r mas	θ deg	$\Delta(x, y)$ mas	a mas	b/a	Φ deg	S mJy
1.6	03-08-07	1.312	A, e	0	0	–	3.29±0.02	0.5	29.6	24.9±1.3
			N1, e	7.61	-130	0.02	6.20±0.04	0.5	-67.3	21.4±1.1
			B, e	10.58	-22	0.05	8.88±0.10	0.6	-14.7	13.1±0.7
			S1, c	14.11	-165	0.35	4.23±0.07	1	-84.2	8.2±0.4
1.6	08-02-26	1.001	A, e	0	0	–	3.29±0.01	0.5	29.6	31.9±1.6
			N1, e	8.08	-128	0.01	6.20±0.02	0.5	-67.3	31.0±1.6
			B, e	10.18	-17	0.02	8.89±0.04	0.6	-14.7	21.4±1.1
			S1, c	16.01	-178	0.03	4.23±0.06	1	-84.2	6.6±0.3

5	97-04-06	1.393	C, e	0	0	–	1.92±0.05	0.3	45.7	7.6±0.4
			A, e	4.02	64	0.15	1.43±0.03	0.9	44.7	10.4±0.6
			N1, e	11.19	-6	0.55	10.38±1.09	0.4	-40.5	2.0±0.2
			B, e	5.19	-130	0.03	2.21±0.06	0.7	30.9	7.3±0.4
			S1, e	9.4	-174	0.43	11.08±0.86	0.3	-30.6	2.7±0.2
5	05-07-27	1.205	C, e	0	0	–	1.92±0.03	0.3	45.7	8.3±0.4
			A, e	4.02	65	0.01	1.43±0.02	0.9	44.7	11.9±0.6
			N1, e	12.04	-4	0.13	10.38±0.25	0.4	-40.5	5.3±0.3
			B, e	5.07	-129	0.02	2.21±0.03	0.7	31.0	8.4±0.4
			S1, e	7.38	-158	0.09	11.08±0.18	0.3	-30.6	8.1±0.4
5	08-02-26	0.946	C, e	0	0	–	1.92±0.03	0.3	45.7	9.3±0.5
			A, e	4.02	64	0.01	1.43±0.02	0.9	44.7	11.5±0.6
			N1, e	11.10	-4	0.13	10.38±0.23	0.4	-40.5	5.9±0.3
			B, e	5.04	-127	0.02	2.21±0.04	0.7	30.9	7.7±0.4
			S1, e	6.85	-150	0.08	11.08±0.15	0.3	-30.6	9.7±0.5

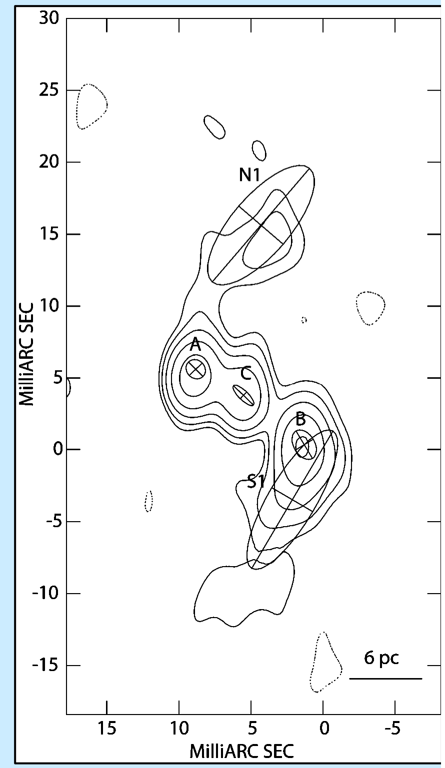

Contour levels= -0.4, 0.4, 0.8, 1.6, 3.2 and 6.4 mJy/b

Peculiar cases of BCGs

4C 26.42 in Abell 1795 (Liuzzo et al. 2009a)

X band

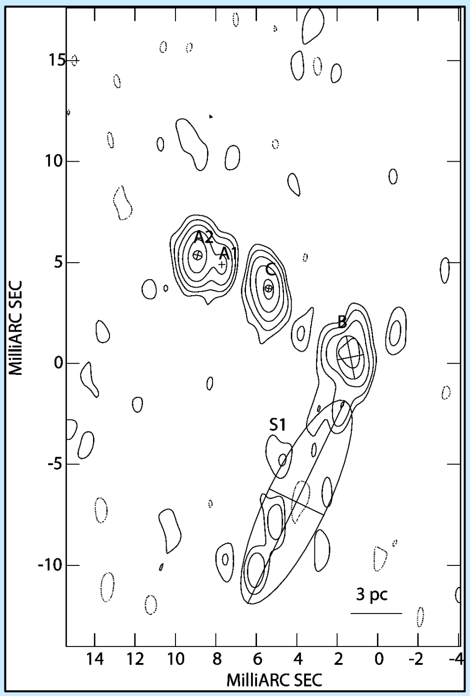

Contour level= -0.25, 0.25, 0.5, 1., 2, 4 mJy/b

Component	r mas	θ deg	Δ (x, y) mas	a mas	b/a	Φ deg	S mJy
C, c	0	0	-	0.34±0.01	1	-11.9	5.3±0.3
A1, d	3.01	61	0.02	0	1	0	2.9±0.2
A2, c	4.02	63	0.01	0.44±0.01	1	-14.7	8.1±0.4
B, e	5.09	-129	0.01	2.21±0.02	0.6	11.0	7.5±0.4
S1, c	8.89	177	0.24	11.08±0.47	0.3	-25.6	1.9±0.1
C, c	0	0	-	0.9±0.03	1	-25.0	4.6±0.3
A1, d	2.05	71	0.01	0	1	0	2.2±0.2
A2, c	4.04	65	0.01	0.15±0.01	1	-21.8	6.8±0.4

Table 4. Spectral index for single component.

ν_1-ν_2 GHz	HPBW mas×mas, °	Component	S_{ν_1} mJy	S_{ν_2} mJy	α
1.6-5	10.0×5.0, 0	A	15.4	7.5	0.63±0.01
		B	29.0	3.6	1.82±0.01
		N1	15.4	6.1	0.82±0.02
		S1	9.4	7.3	0.66±0.03
5-8.4	3.0×3.0,0	A	6.7	6.7	0.00±0.05
		C	4.1	4.1	0.00±0.05
		B	6.2	3.7	1.03±0.06
		S1	7.7	2.6	2.12±0.06
8.4-22	1.86×0.86,-4	C	5.3	4.6	0.14±0.04
		A1	2.9	2.2	0.29±0.08
		A2	8.1	6.8	0.18±0.03

S_{ν_1} and S_{ν_2} are referred to the flux density at lower ν_1 and higher ν_2 frequency between the two considered for the spectral analysis. All flux density values are derived from 2008 February 26 observations.

K band

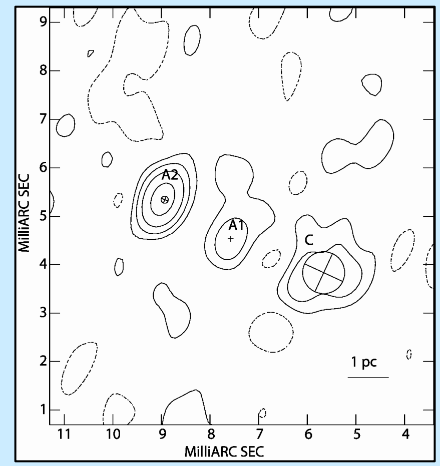

Contour levels= -0.45, 0.45, 1.2, 2.4, 4.8 mJy/b

- Core identification
- S~ $\nu^{-\alpha}$ → asymmetric interaction with the surrounding medium
- No proper motion→ standing shocks

Peculiar cases of BCGs

4C 26.42 in Abell 1795 (Liuzzo et al. 2009a)

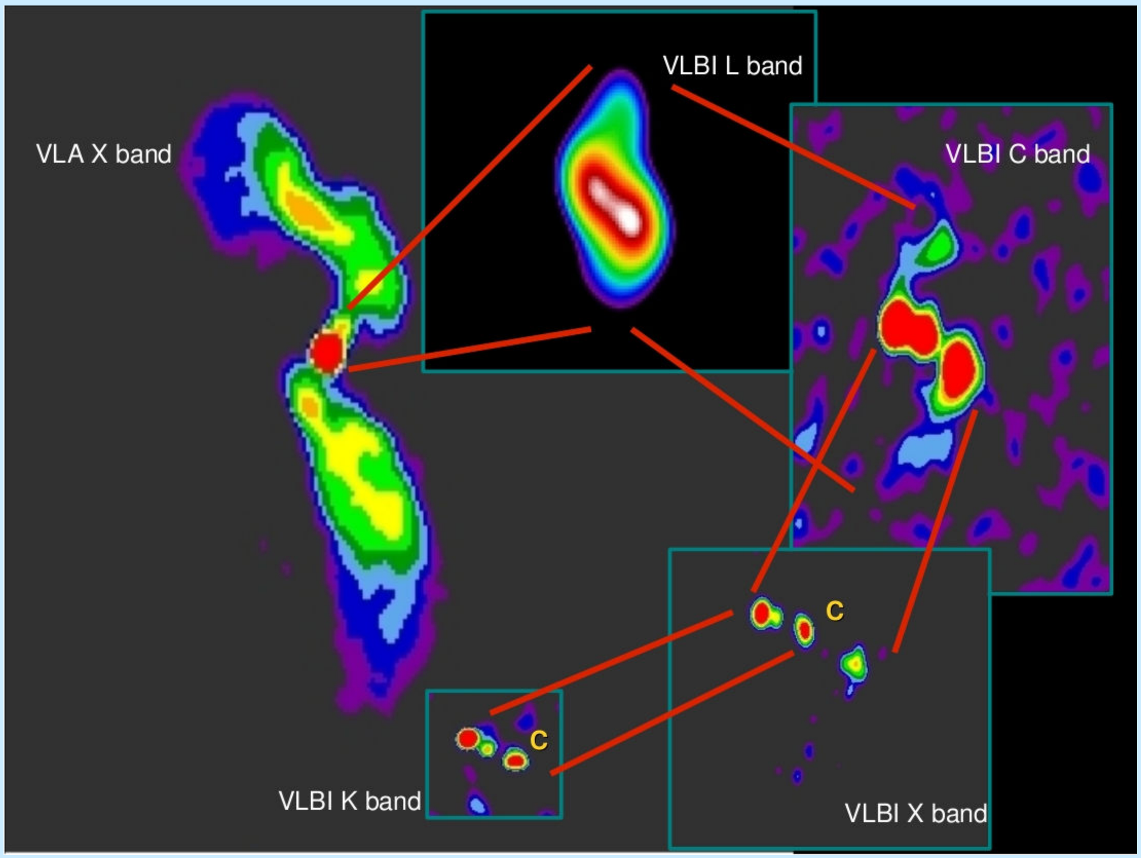

• **2 dramatic changes in P.A**:

-2 arcsec :
a) rotating disk?
(3C 293 →
Van Breugel et al. 1984)
b) buoyancy?
(Fabian et al. 2001)

-5 mas :
a) BBH?
(Merritt et al. 2002)

or → rotating vortices?
(Forman, 2009→A115)
or→ complex gas?
(Augusto, 2009→A2390)

Peculiar cases of BCGs

NGC6047 in Abell 2151

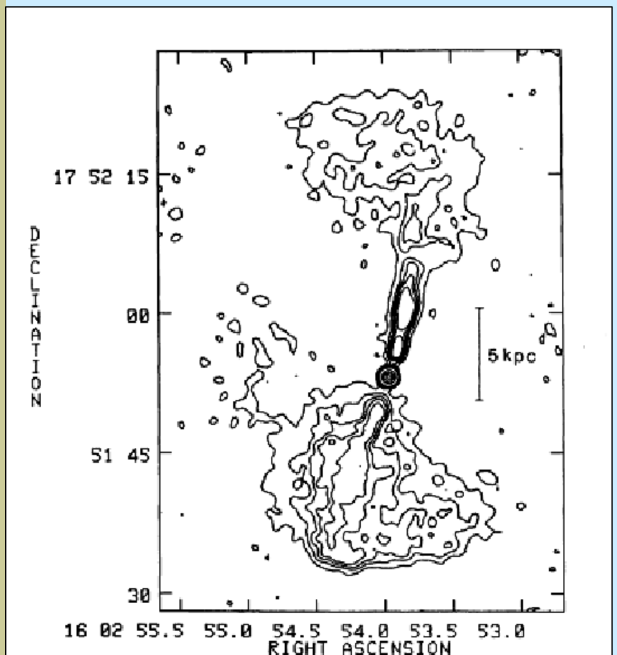

6cm VLA map (Feretti & Giovannini 1988): Contour levels from 0.1 to 7 mJy/beam.

Need of deeper observations (e.g EVN) to properly map parsec structured core emission

→A2151 (Hercules cluster) is an **ongoing cluster merging** with two main condensation : NGC6041A is BCG for the 1st and NGC6047 for the 2nd .(Girardi et al. 2007) .

→ NGC 6047 is an E/SO with evidence of **recent merger** (Dickey 1997)

→ *kpc radio morphology*:

Extended FRI with the northern jet brighter (flux at 5 GHz = 13.6 mJy) and more collimated.
Total flux at 1.4 GHz is 728 mJy
Core flux density at 5 GHz is 8.3 mJy
Core dominance < 0.47

→ *pc scale morphology*

- **5 GHz** VLBA map (2008) : undetected above $5\sigma = 0.55$ mJy/beam

- **new 1.6 GHz** VLBA observations (July 2010., 16 x 11 mas) **undetected** above $5\sigma = 0.5$mJy/beam

- non detection due to: radio quiet core? excluded
core coordinates? excluded
diffuse core emission? To check

Peculiar cases of BCGs

IC712 in Abell 1314

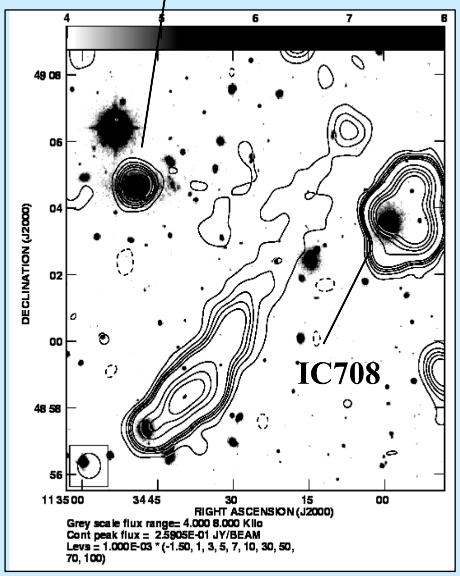

NVSS (contours) + optic

→ IC 712 is the BCG of the main condensation

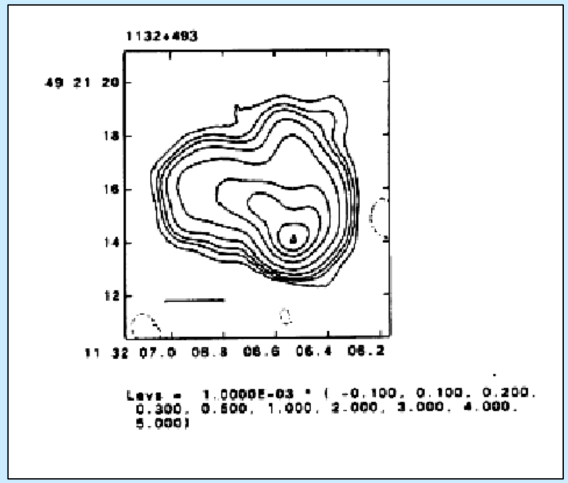

1.4 GHz VLA image (Feretti & Giovannini (1994))
Contour levels are from 0.1 to 5 mJy/beam

→ *kpc scale morphology:*

- **WAT** structure with small angular size (< 4.5 arsec) (Feretti & Giovannini 1994)
- Total flux: 26.3 mJy at 1.4 GHz
- Core flux 14.02 mJy at 5 GHz
- Core dominance = 4.37

→ *pc scale morphology*

- **5 GHz** VLBA map (2008) : undetected above 5σ = 0.45 mJy/beam

- **new 1.6 GHz** VLBA observations (July 2010, 16 x 10 mas): **undetected** above 5σ =0.5.mJy/beam

parsec structured core emission needs deeper observations (e.g EVN) to be properly mapped

3C 84 in A426

Refer to talk of K.Kellermann…

Chandra + 1.4 GHz VLA

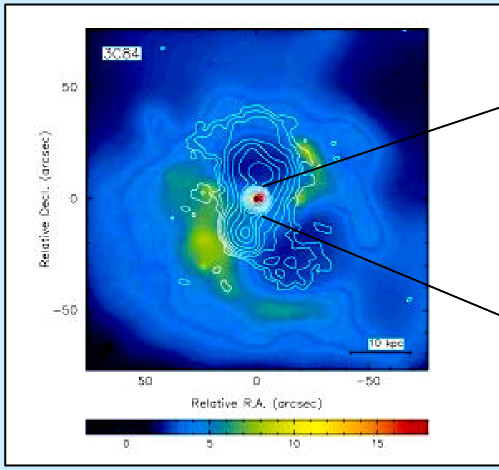

VLBA 330 MHz

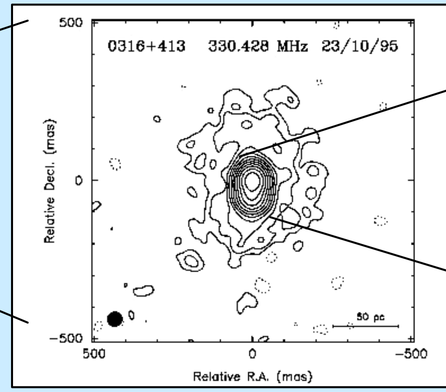

VLBA 5 GHz

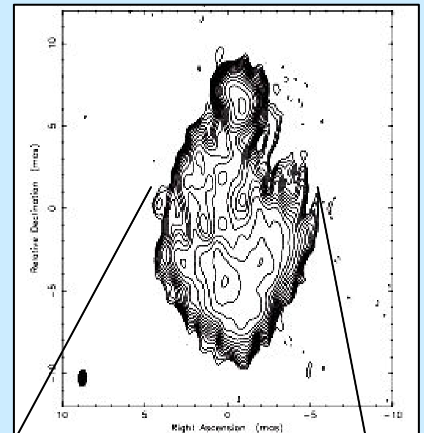

VLBA 43 GHz

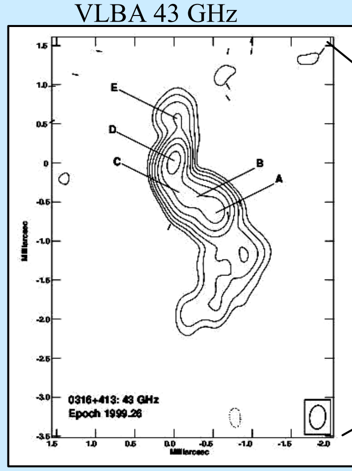

VLBA 22, 15, 8.4 and 5 GHz

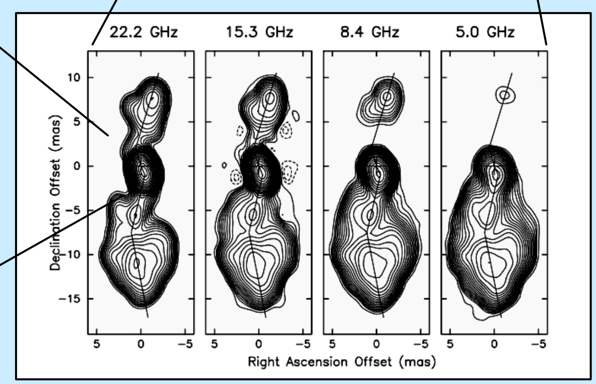

- cool core cluster
- cD galaxy NGC1275
- RM ~ 7000 rad/m^2 (Taylor et al. 2006)
- outburst in the 1959 (Asada et al. 2009)
- ‘millihalo’ (Taylor et al. 1998)
- free-free absorption (Walker et al.2000)

Notes:

cool core cluster + restarted activity + mildly relativistic jets

Results for the extended sample

(Liuzzo et al. 2010)

Cluster morphology	#	two-sided	one-sided	point	N.D.
BCG in relaxed clusters:	10	**7 (70%)**	-	1 (10%)	2 (20%)
BCG in merging clusters:	22	-	**13 (59%)**	1 (5%)	8 (36%)

Strong dichotomy

From conclusions for BCS sample (Giovannini et al. 2003, 2005, Liuzzo et al. 2009)
→ 1s is predominant and only 22 % of FRI radio galaxy have 2s jets.

In agreement with expectations based on a random orientation for sources with relativistic jets
All FRIs in non cool core clusters have similar pc scale properties regardless their host galaxy classification
(BCGs or not BCGs)

One sided structures in non cool core clusters are due to Doppler boosting effects in relativistic, intrinsically symmetric jets

Conclusions

Jet velocity for two-sided morphology

Two sided structures can be due to → relativistic jet in the plane of sky

NO for our BCGs

due to statistical consideration in comparison with BCS

→ In cool core clusters 2s are 70% versus 22 % in BCS sources

→ mildly relativistic jets

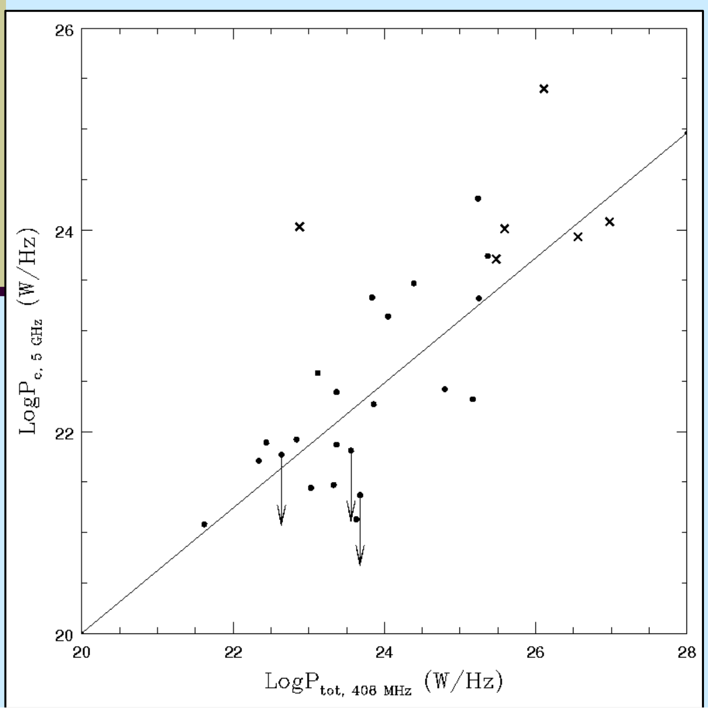

BCGs in cool core clusters are not in agreement with the correlation of Giovannini et al. 2001

Solid line → correlation found by Giovannini et al. 2001 for randomly oriented sources with relativistic jets

↓ Radio quiet core

x for BCGs in cool core clusters

• for BCGs in non cool core clusters

N.B.: 2s structures only in clusters with Mass accretion rate > 90 M_{sol}

Conclusions

Mildly relativistic jet: the model of Rossi et al. 2008

Rossi et al. 2008 show that a jet perturbation grows because of K-H instability and produce a

strong interaction between the jet and the surrounding medium with a consequent jet deceleration.

Taking Lorentz factor equal to 10 and exploring the parameter plane **(M, η)** ,
where M is the Mach number and η is density ratio between the surrounding medium and the jet,
they found that η plays the fundamental role in the deceleration of jet.

In FR I relativistic jets slow down on the sub-kpc scale

In BCG in cooling clusters relativistic jets could slow down on the pc (sub-pc) scale (→e.g. 3C 84)

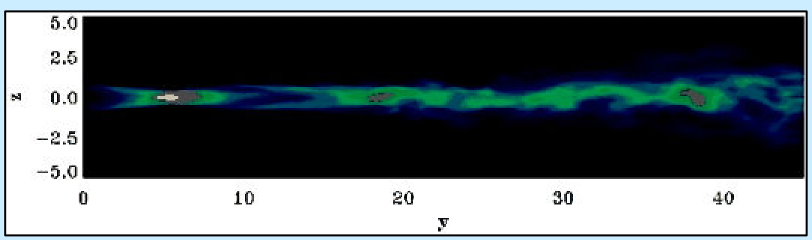

Simulated map:
M=3 , $\eta = 10^4$, $\theta = 20^0$ is the direction of the jet

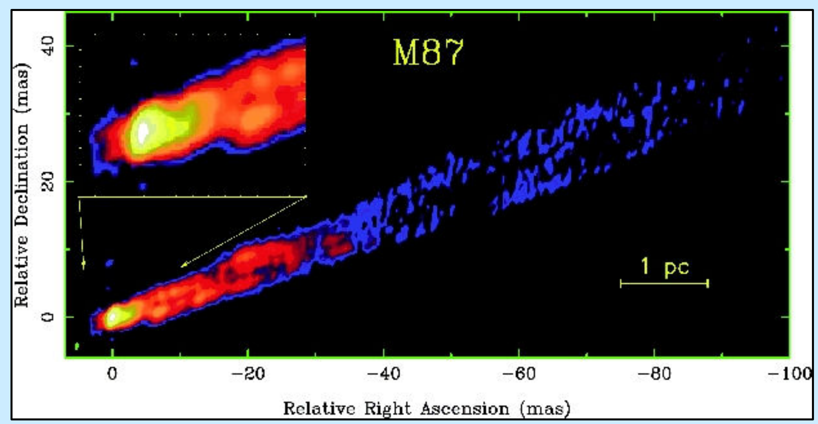

VLBA map at 2 cm

Conclusions

(Liuzzo et al. 2010)

- BCGs are **unique class** of objects

- To study their pc scale properties we define a **complete sample** taking BGCs in all Abell cluster with DC<3 and declination > 0

- To better understand we added other BCGs → **extended sample** = 34 BCGs

- **Complex structure** in the radio core have been found at parsec scale.

- Complex structure need **deeper VLBI observations → EVN observations**

- a **clear dichotomy** is found: → 56% of BCGs in non cool core clusters have 1s jets
→ 54% of BCGs in cool core clusters show 2s jets

-Using the BCS sample as comparison sample, we suggest
→ 2s jets are due to **mildly relativistic** jets in cool core clusters

-The strong interaction with the **dense surrounding medium** plays the main role in the jet velocity deceleration in BCGs in non cool core clusters

- Evidences of **restarted radio activity** in cool core clusters are of great interest to the study of AGN feedback in clusters.

References: Liuzzo et al. 2009a A&A, 501, 933L
Liuzzo et al. 2009b A&A, 505, 509L
Liuzzo et al. 2010 Astroph 1002.1380

Thank you

Man on the Wall (Lowry, L.S., Manchester)

Peculiar cases of BCGs

IC708 in Abell 1314

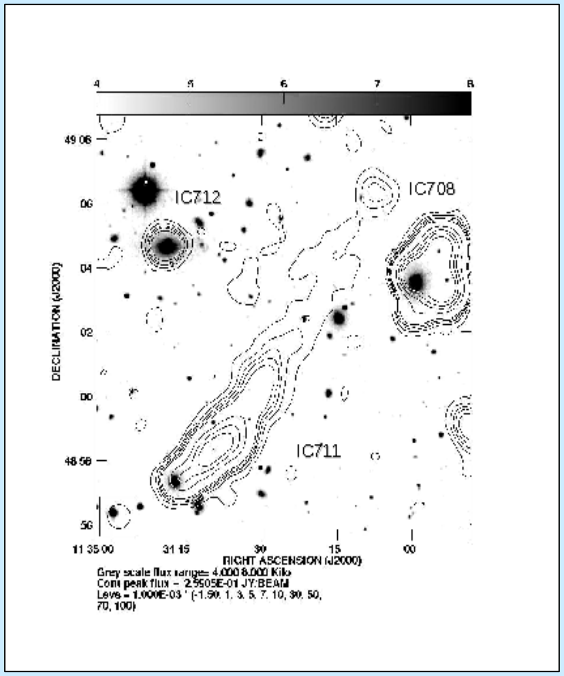

NVSS

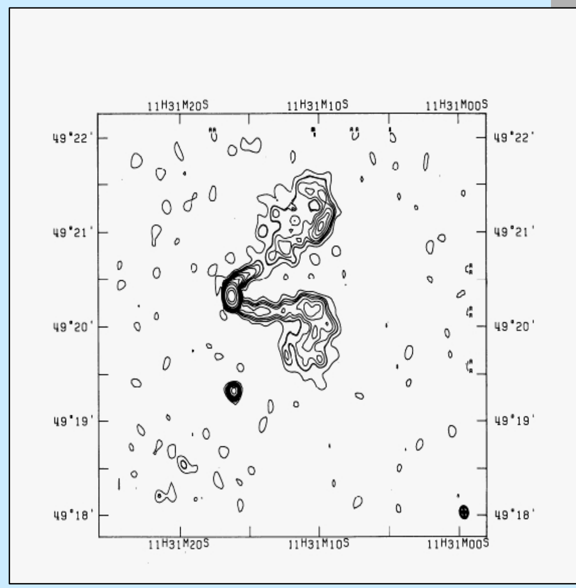

1.4 GHz VLA

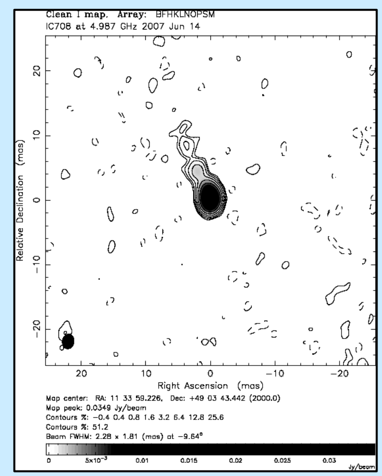

5 GHz VLBA

IC 708 is the BCG of the second condensation.

It also shows a WAT structure (Vallee et al. 1979) with a larger size (4.5 arcsec), total flux density at 1.4 GHZ of 430 mJy and core flux density at 6 cm of 110 mJy.

In our maps, IC 712 is undetected at the 5σ level (<0.45 mJy/ beam).
IC 708 shows a one-sided structure with a core flux density S of 38.8 mJy.
The jet is aligned with the kiloparsec structure, has S of 2.48 mJy and an extension of 16 mas from the core.

Peculiar cases of BCGs

NGC6047 in Abell 2151

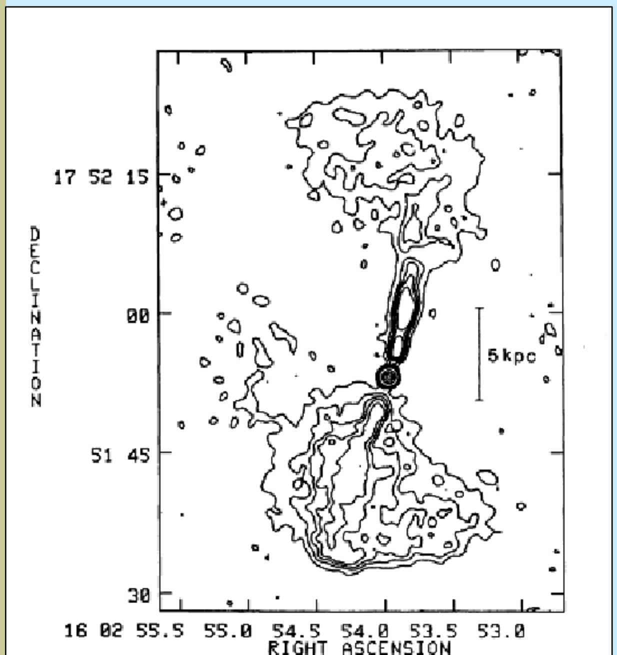

6cm VLA map (Feretti & Giovannini 1988):
Contour levels from 0.1 to 7 mJy/beam.

Need of deeper observations (e.g EVN) to properly map parsec structured core emission

→A2151 (Hercules cluster) is an **ongoing cluster merging** with two main condensation : NGC6041A is BCG for the 1st and NGC6047 for the 2nd .(Girardi et al. 2007) .

→ NGC 6047 is an E/SO with evidence of **recent merger** (Dickey 1997)

→ *kpc radio morphology*:

Extended FRI with the northern jet brighter (flux at 5 GHz = 13.6 mJy) and more collimated.
Total flux at 1.4 GHz is 728 mJy
Core flux density at 5 GHz is 8.3 mJy
Core dominance < 0.47

→ *pc scale morphology*

- **5 GHz** VLBA map (2008) : undetected above 5σ = 0.55 mJy/beam

- **new 1.6 GHz** VLBA observations (July 2010): **undetected** above 5σ = ….mJy/beam

- non detection due to: radio quiet core? excluded
  core coordinates? excluded
  diffuse core emission? To check

Peculiar cases of BCGs

NGC6041A in Abell 2151

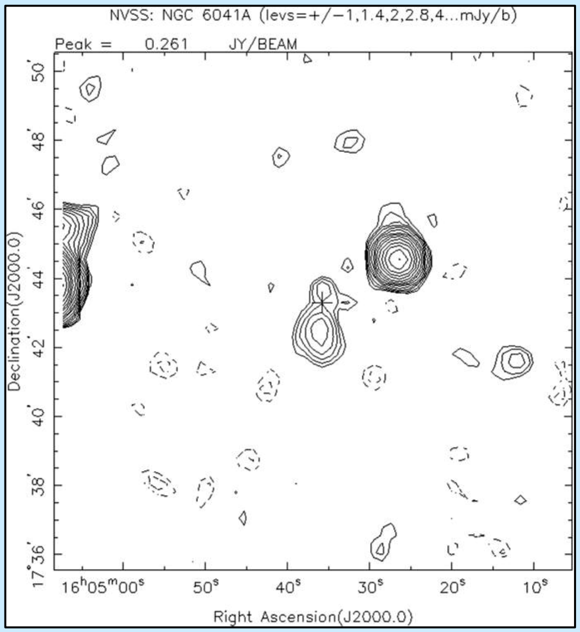

NVSS

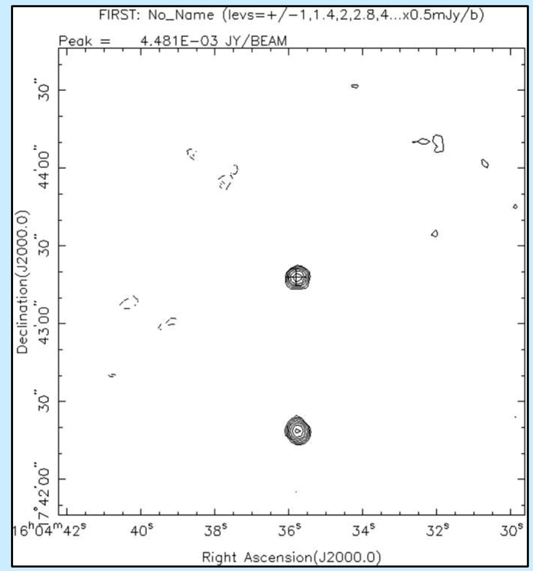

FIRST

NGC 6041A is the BCG of the first main condensation .

In the NVSS image, NGC 6041A shows a WAT structure with angular size of 2.5 arcmin and total flux density of 11.6 mJy.

In our VLBA map, it appears unresolved with a total flux density of 7.83 mJy.

Parsec scale properties of BCGs (Liuzzo et al. 2010)

Unresolved and undetected sources

Unresolved sources: 1) NGC 708 in cool core cluster A262 → core dominance very low (0.25)
→ low phase of nuclear actvity

2) NGC6041A in merging cluster A2151 → faint source
(LogP = 22.57 W/Hz at 1.4 GHz)
→ sensitivity?

Undetected sources: - radio quiet sources (5/11)

- radio quiet core (4/11) (e.g. NGC6086 relic rs) → core dominance low

- peculiar sources (2/11) : NGC 6047 and IC 712 → extremely core variability?
complex structures?
need of more observations…

VLBA observations

General properties of BCGs

Radio Loud BCGs

Cooling Flow problem

Radio loud BCGs has been proposed as a potential solution to the cooling flow problem.

(Fabian et al. 1994)

- Some problems…balance? One episode of radio-loud? Duty cycle?

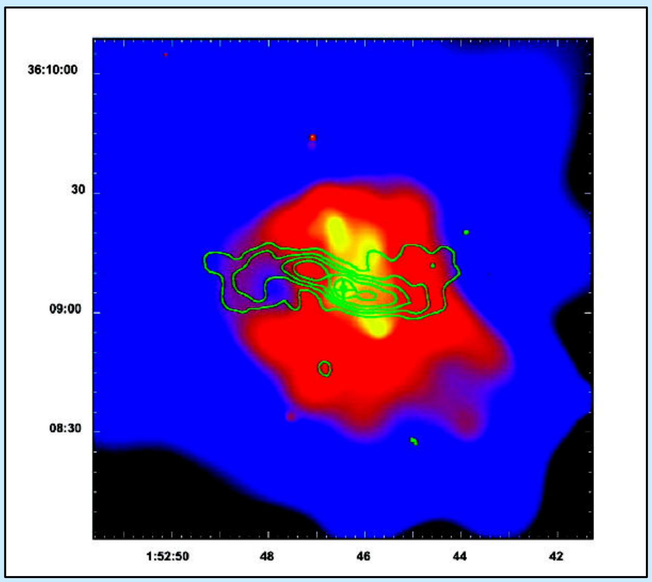

A262 (Blanton et al. 2004)
→ balance of cooling losses

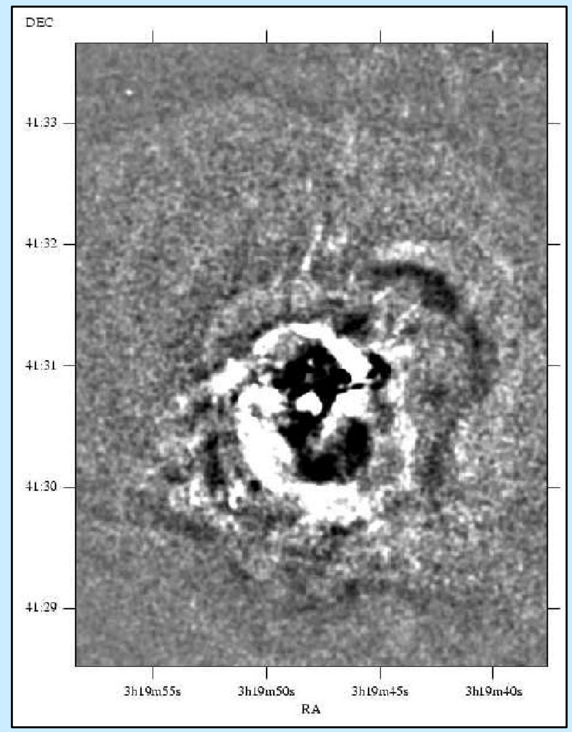

‘Ripples’ in Perseus cluster
(Fabian et al. 2003)

Parsec scale properties of BCGs (Liuzzo et al. 2010)

Statistical considerations

* *Detection rate*

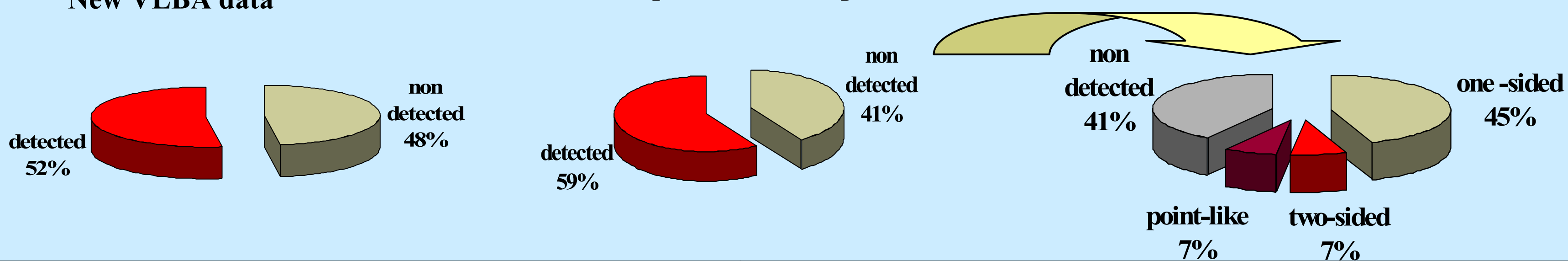

* *Cluster dynamics*

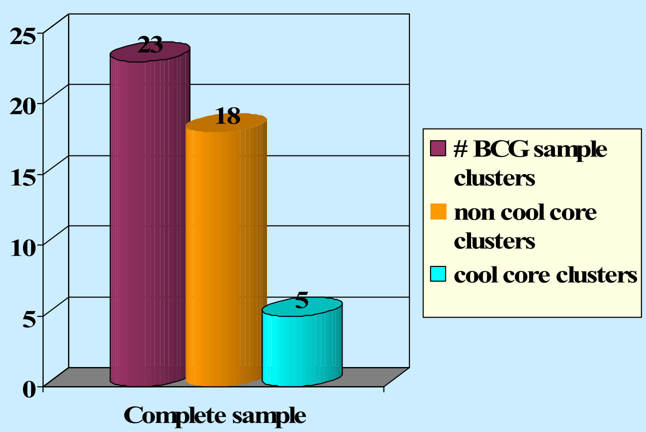

- 22% of cool core clusters

* S_{VLBI} / S_c *(%)*

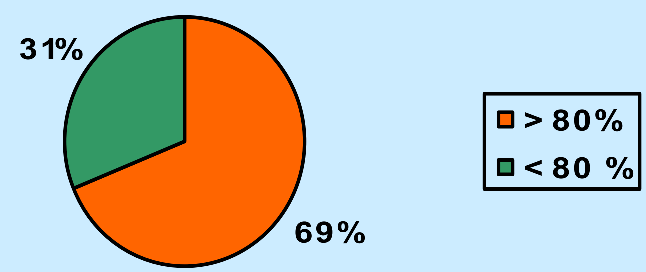

Good mapping of the most of mas scale structure parsec scale

Variability? Significant structures at sub arcsec scales
→ More observations…

Parsec scale properties of BCGs (Liuzzo et al. 2010)

Statistical considerations

*** *Evidence of Restarted Activity***

3C 84 and 3C 338 → In cool core clusters

3C 84:
Nagai et al. 2009,Agudo et al. 2005

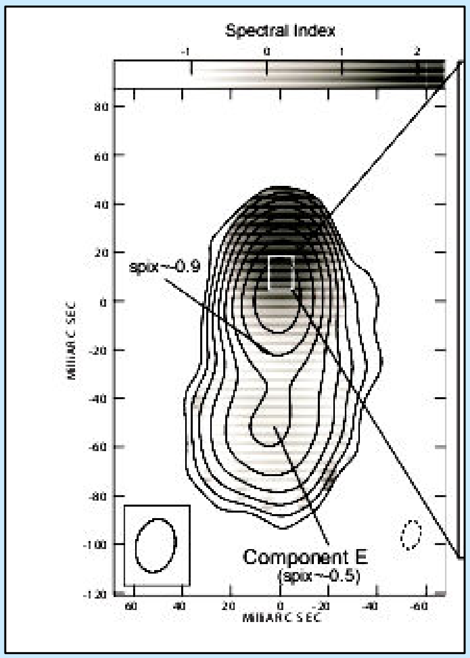

Synchrotron
and kinematic
Age→
15 mas: outburst 1959
100 mas: older

3C 338:
Giovannini et al. 1998

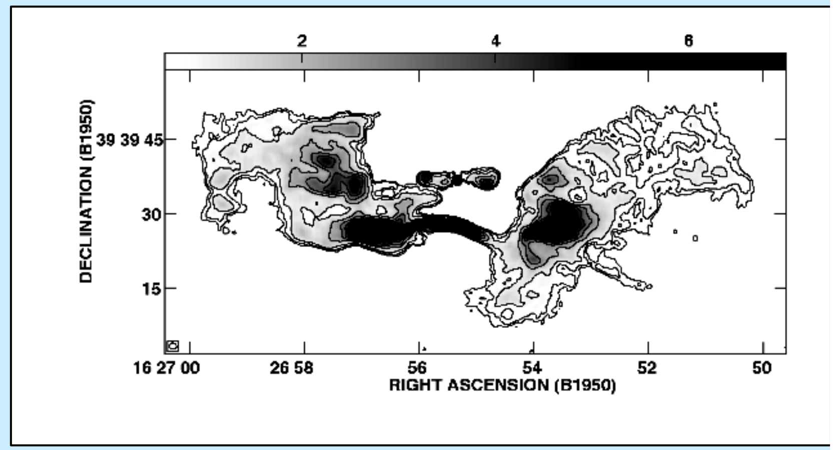

Morphology, variability → diffuse region
Is a old relic radio emission

Great interest to the cooling problem (McNamara et al.2005) →
BCGs in cool core clusters heating source of ICM

Parsec scale properties of BCGs (Liuzzo et al. 2010)

Statistical considerations

* ***kpc morphologies***

- Non cool core clusters

→Wide Angle Tail (Owen et al. 1985)

→ All one sided at pc scale

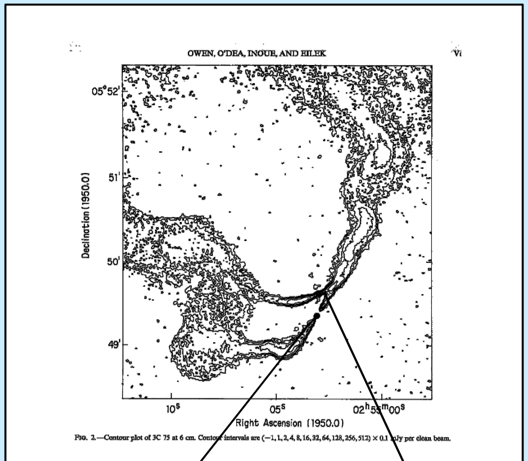

3C 75 in A400

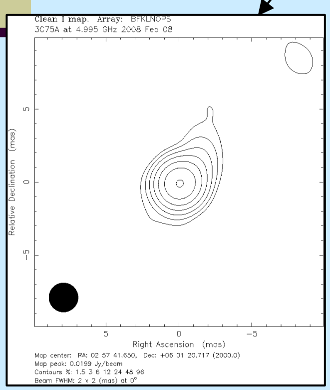

3C 75A

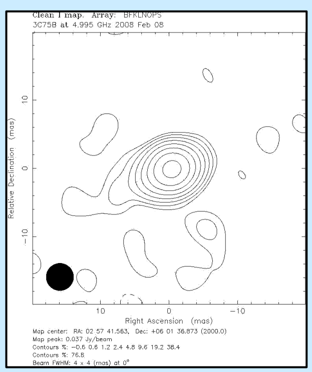

3C 75B

- Cool core clusters

→core + halo radiosource (Owen et al. 1990)

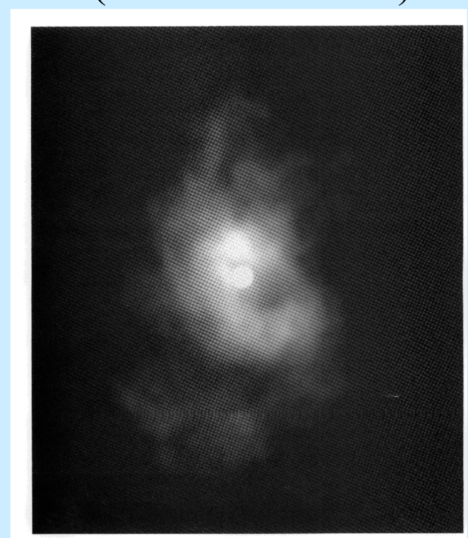

3C317 in A2052

20 cm VLA

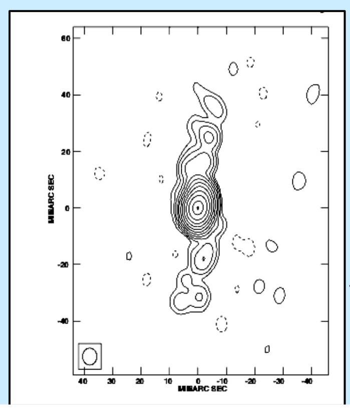

1.7 GHz VLBA

5 GHz VLBA

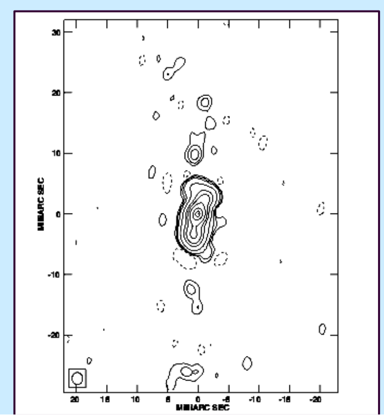

Peculiar cases of BCGs

Hydra A in Abell 780

- Cool core cluster with $L_X \sim 2 \times 10^{44}$ erg/s (David et al. 1990)

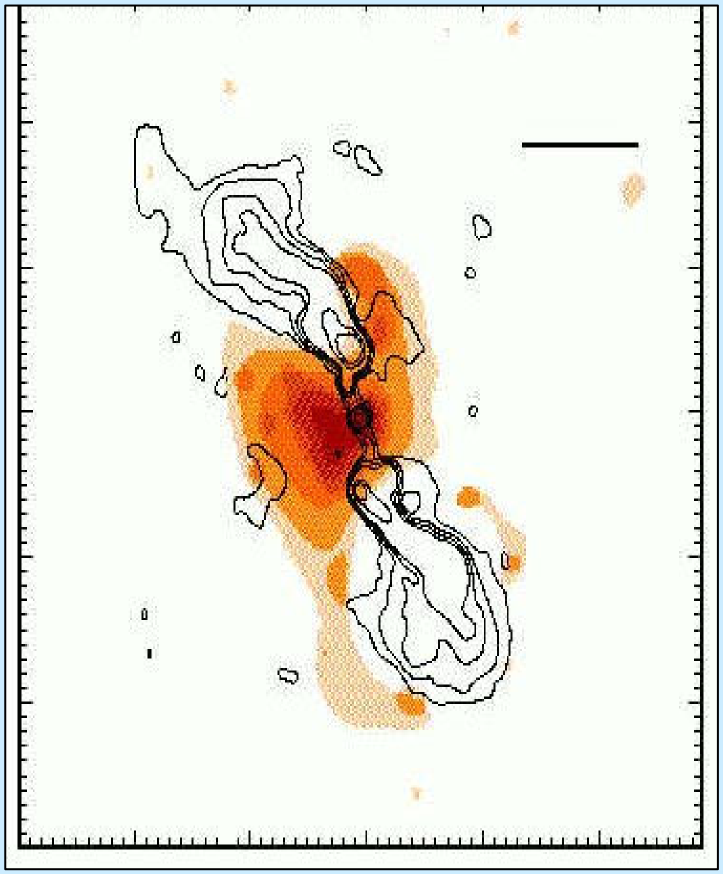

CHANDRA + VLA

- cD multiple nuclei
- disk of gas
  (Dimkim 1979)

- FRI/FRII
- S shape
  → precession
  (Taylor et al. 1990)
- RM > 8000 rad m^{-2}
  (Taylor et al. 1993)

- At pc scale: 2s

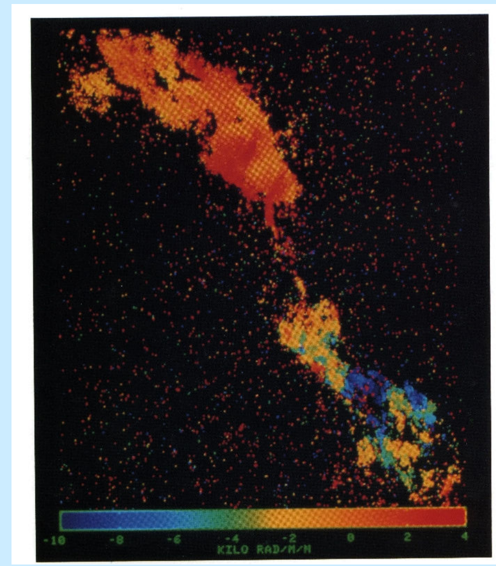

RM

1.3, 5 and 8 GHz VLBA

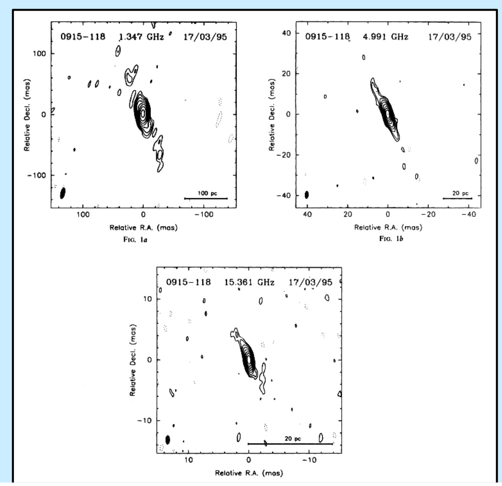

The comparison sample : Bologna Complete Sample

The definition of BCS sample

(Giovannini et al. 1990, 2001, 2005, Liuzzo et al. 2009b)

The aim: parsec scale study of statistical properties in different class of sources

The method : definition and observations of sample free from selection effects looking at low frequences samples

If $S \sim \nu^{-\alpha} \rightarrow S(app)= S(true)D^{2+\alpha}$ where $D = \frac{1}{\Gamma(1-\beta\cos\theta)}$

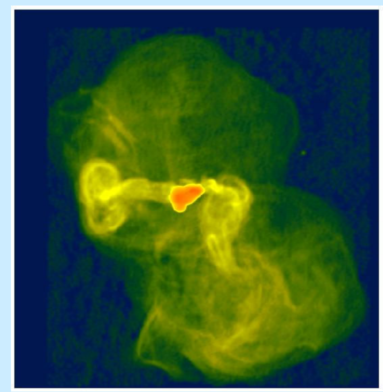

M87 VLA 90 cm

The sample: → 94 sources (53 studied)

→ B2 catalog and 3CR catalog with no contraint on nuclear properties

→ Criteria:

1) flux density limit > 0.25 Jy at 408 MHz for the B2 and 10 Jy at 708 MHz for 3CR
2) declination > 10 deg
3) galactic latitude $|b| > 15^0$
4) redshift $z < 0.1$

The data: - in this PhD project → 23 sources with $S_{c,\,VLA}$ >5 mJy at 5 GHz and 1.6 GHz for 10 sources

- 2010 February EVN and VLBA proposal for the remaining 18 sources

The comparison sample : Bologna Complete Sample

Source morphology

(Giovannini et al. 1990, 2001, 2005, Liuzzo et al. 2009b)

* **Representative sample** In a randomly oriented sample:

$P(\theta_1, \theta_2) = \cos\theta_1 - \cos\theta_2$ → In BCS P(FRI+FRII) = 84% → $\theta = 33^0$ → ok

* **Kiloparsec structures**
  among sources with VLBA data

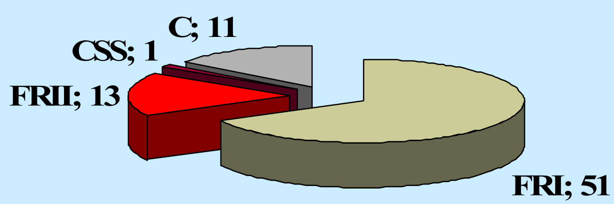

* **C source pc morphologies**

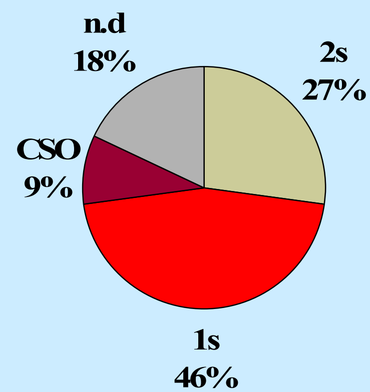

→ low power compact sources have sub-kpc structure

* **FRII brighter than FRI** →27 % of FRI and 46% of FRII are two sided

The comparison sample : Bologna Complete Sample

Source morphology

(Giovannini et al. 1990, 2001, 2005, Liuzzo et al. 2009b)

* **No correlation** between j/cj and P(core, VLA) or P(tot)

* kpc structure **aligned** with pc scale structure (e.g .4C 29.30)

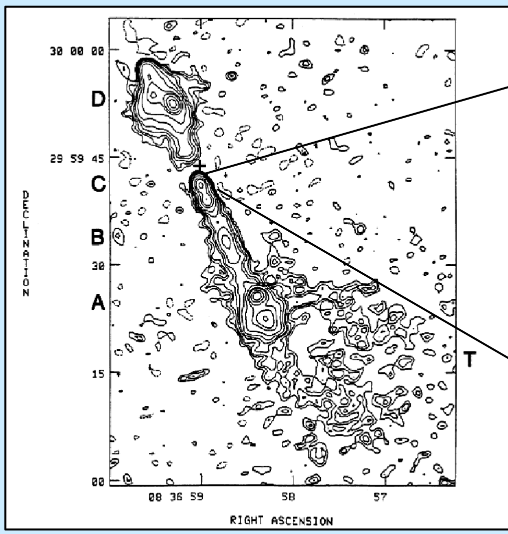

6 cm VLA

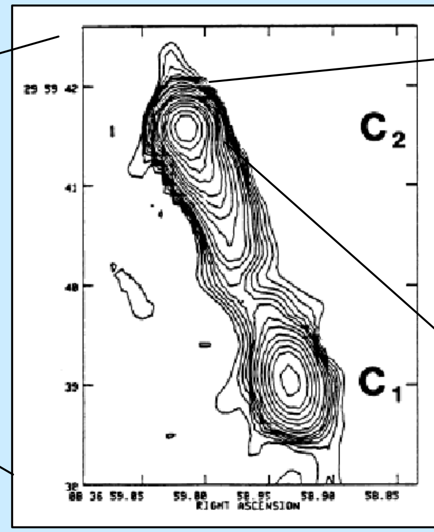

5 GHz VLBA

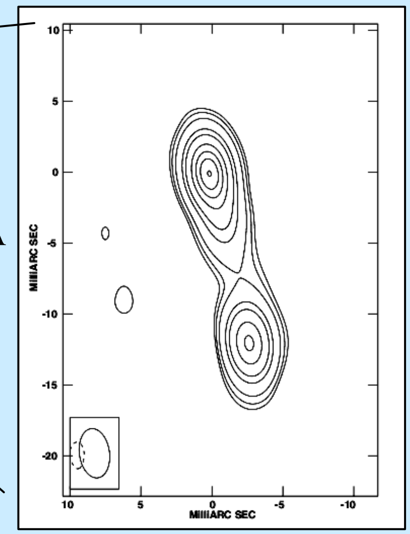

Missing flux in pc scale structures → S_{VLBI} / S_c (%)

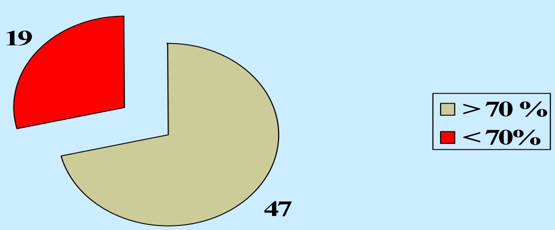

Good mapping of the most of mas scale structure parsec scale

Variability? Significant structures at sub arcsec scales → More observations…

The comparison sample : Bologna Complete Sample

Source morphology
(Liuzzo et al. 2009b)

* **<u>Doppler boosting effects</u>** → 41% of sources are one -sided

* **<u>Unresolved sources:</u>** 20% (15 sources)
→ 14 FRI and 1 FRII → faint relativistic jets in the plane of sky

* 4% (1 FRI and 2 C-shaped) of new observed sources are **non detected**

* **<u>2 Z –shaped sources</u>** →3C 310 and 4C 26.42→ 2s on pc scale → mildly relativistic jets

3C 310

20 cm VLA

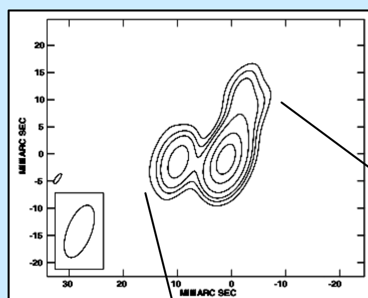

1.6 GHz VLBA

5 GHz VLBA

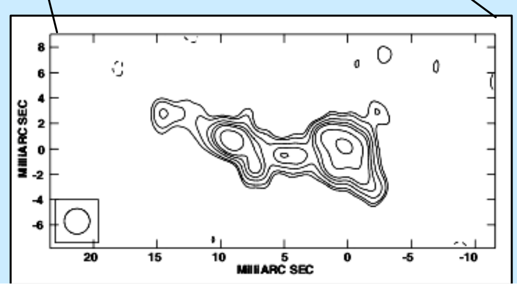

Spectral index map

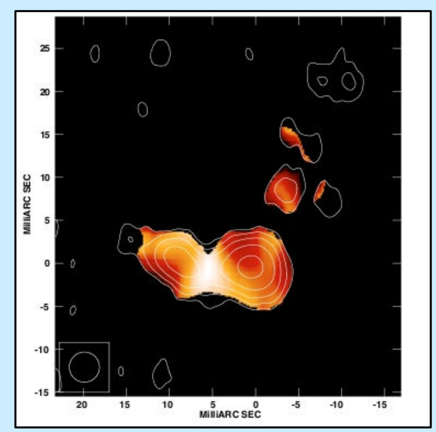

- 0.3 8(white)→ 2 (dark red)

The comparison sample : Bologna Complete Sample

Jet velocity and orientation

(Giovannini et al. 1990, 2001, 2005, Liuzzo et al. 2009b)

• $\mathbf{S_J / S_{cJ}} \geq 10$

→ 1s → (not for 0055+30 and 0220+43 → CJ detection)

relativistic jets

•**Core dominance**: $P_{(core,\ observed)} / P_{(core,\ estimated)}$

where $\log P_{(core,\ estimated)} = 0.62 \log P_{(tot,\ 408MHz)} + 7.6$ ($\theta = 60$) (Giovannini et al. 1994)

for BCS:
core dominance

>1 → $\theta < 60^0$
0.25-1 → $\theta > 60^0$ → deboosting
>> 1 → restarted activity?
(2 BL Lacs and 0222+36 have >10)
< 0.25 → no solution → nuclear variability
→ low radio phase
(4 FRI + 4 narrow line extended and powerful FRII)

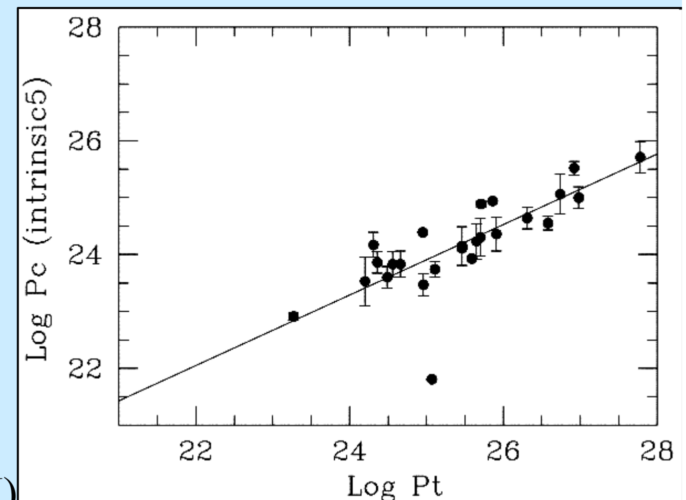

Conclusions

Bologna Complete Sample	versus	Brightest Cluster Galaxies sample
-Detection rate high : 97 %		-Detection rate 60 % → 76% with only radio loud BCGs at kpc scale
- 1s predominant on pc scale → random orientation and high jet velocity		- ***dichotomy* on pc scale structure → 1s in BCGs in non cool core clusters 2s in BCGs on cool core clusters**
- 2 Z-shaped → low velocity jets		- 1 Z-shaped → low velocity jets
- 10 % low radio activity state → restarted sources		- 2 evidences of restarted sources and 4 of radio quiet core in radiogalaxies
-kpc and pc structures aligned		- kpc and pc structures aligned
- 38% of sources evidence of core variabilty or sub-kpc structures		- 30% of sources evidence of core variabilty or sub-kpc structures

- Similar pc morphologies (some cases of sub-kpc structure)
- intermittent activity
- **only one-sided BCGs have similar kinematic properties with FRIs**

Conclusions

Mildly relativistic jet: the model of Rossi et al. 2008

Rossi et al. 2008 show that a jet perturbation grows because of K-H instability and produce a

strong interaction between the jet and the surrounding medium with a consequent jet deceleration.

Taking Lorentz factor equal to 10 and exploring the parameter plane **(M, η)** ,
where M is the Mach number and η is density ratio between the surrounding medium and the jet,
they found that η plays the fundamental role in the deceleration of jet.

In FR I relativistic jets slow down on the sub-kpc scale

In BCG in cooling clusters relativistic jets could slow down on the pc (sub-pc) scale (→e.g. 3C 84)

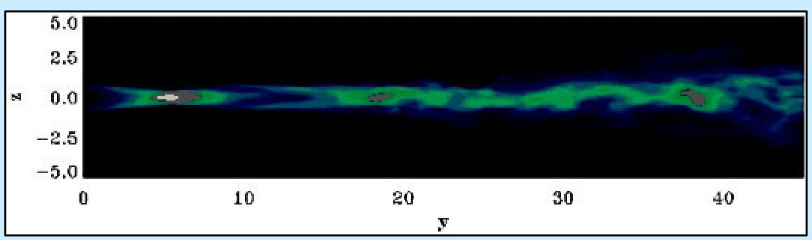

Simulated map:
M=3 , $\eta = 10^4$, $\theta = 20^0$ is the direction of the jet

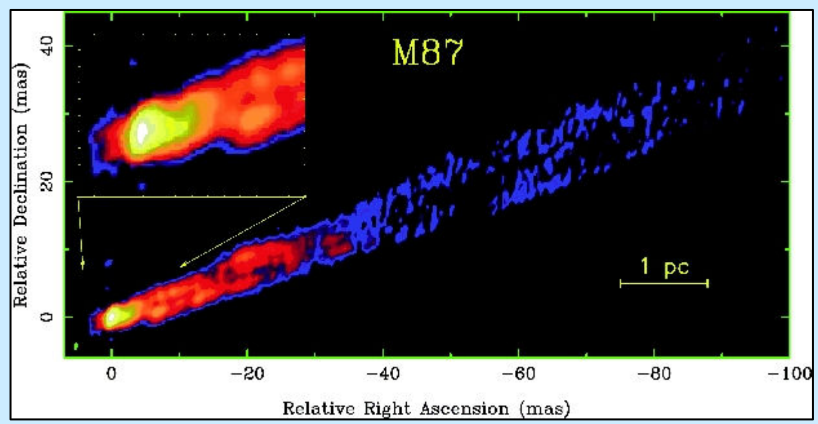

VLBA map at 2 cm

Conclusions

Dense surrounding medium in cool core clusters

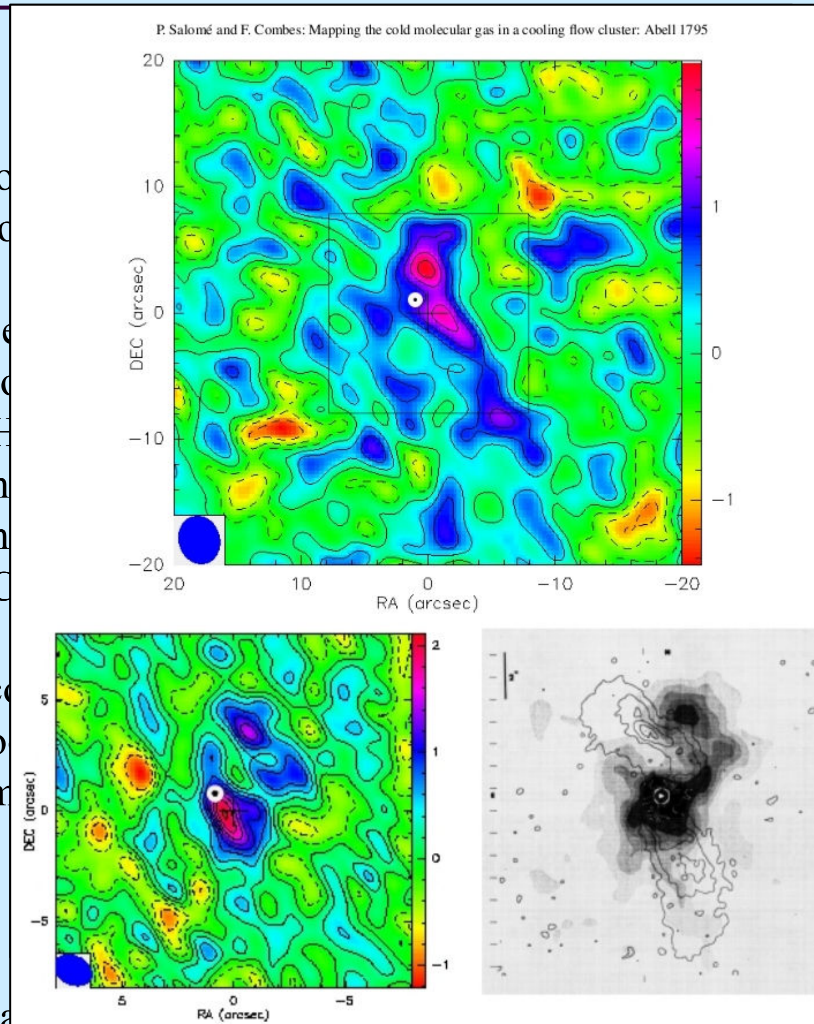

- X-ray cavities → sc
  → co
- ICM multiphase (Fe
  → ic
  → H ord & Fabian (1992))
  → n ea et 1998)
  → h s, Edge et al. 2002)
  → C
- Notes on pc scale co
  → co
  → sm de et al.2008)

the warm gas tha ation on (sub)pc scale

Abell Cluster	cool core	M_{acc} $M_{\odot}/yr$	BCG	Large scale	VLBI	Ref.
A400	N	$0.0^{+28.3}_{-0.0}$	3C75A	WAT	one sided	White et al. (1997)
	N	$0.0^{+28.3}_{-0.0}$	3C75B	WAT	one sided	White et al. (1997)
A407	N	$4.6^{+11.8}_{-4.6}$	UGC2489	Tail rs	one sided	White et al. (1997)
A539	N	$2.1^{+6.8}_{-2.1}$	UGC3274	radio quiet	n.d.	White et al. (1997)
A569	N	$>5.2^{+0.0}_{->4.2}$	NGC2329	WAT	one sided	White et al. (1997)
A576	N	17^{+47}_{-17}	CGCG261-059	Tail rs	one sided	White et al. (1997)
A690	N	$0.0^{+15.3}_{-0.0}$	B2 0836+29 II	WAT	one sided	Giovannini et al. (2005); White et al. (1997)
A779	N	$3.1^{+1.1}_{-1.1}$	NGC2832	radio quiet	n.d.	White et al. (1997)
A1185	N	$0.0^{+1.5}_{-0.0}$	NGC3550	radio quiet	n.d.	White et al. (1997)
A1213	N	$0.0^{+11.5}_{-0.0}$	4C29.41	FRI	one sided	White et al. (1997)
A1228	N	—-	IC2738	radio quiet	n.d.	-
A1314	N	$0.0^{+3.0}_{-0.0}$	IC708	WAT	one sided	White et al. (1997)
	N	$0.0^{+3.0}_{-0.0}$	IC712	small WAT	n.d.	White et al. (1997)
A1367	N	$2.3^{+6.8}_{-2.3}$	NGC3842	small WAT	n.d.	White et al. (1997)
	N	$2.3^{+6.8}_{-2.3}$	3C264	HT	one sided	Lara et al. (1999); White et al. (1997)
A1656	N	$0.0^{+1.0}_{-0.0}$	NGC4874	small WAT	one sided	White et al. (1997)
A2147	N	$0.0^{+14.5}_{-0.0}$	UGC10143	small WAT	n.d.	White et al. (1997)
A2151	N	$6.3^{+26.3}_{-3.2}$	NGC6041	small WAT	core	White et al. (1997)
	N	$6.3^{+26.3}_{-3.2}$	NGC6047	compact core+symmetric jets	n.d.	White et al. (1997)
A2162	N	—-	NGC6086	FRI, relic source	n.d	-
A2197	N	$2.4^{+3.0}_{-2.4}$	NGC6173	point source	one sided	White et al. (1997)
A2634	N	$0.0^{+1.5}_{-0.0}$	3C465	WAT	one sided	Venturi et al. (1995); White et al. (1997)
A2666	N	$0.0^{+2.6}_{-0.0}$	NGC7768	Tail rs	one sided	White et al. (1997)
A3526	N	$5.2^{+0.3}_{-0.3}$	PKS 1246-410	small tailed rs	one-sided	Taylor et al. (2006); Hudson et al. (2009)
A262	Y	$9.4^{+21.2}_{-4.4}$	NGC708	double-no core,jets	core	White et al. (1997)
A347	SCF	$7.8^{+3.5}_{-2.7}$	NGC910	radio quiet	n.d.	White et al. (1997)
A426	Y	291^{+2-7}_{-58}	3C84	Compact core+Halo	two sided	Taylor et al. (2006b); White et al. (1997)
A780	Y	222^{+58}_{-132}	Hydra A	double	two sided	Taylor (1996); White et al. (1997)
A1795	Y	321^{+166}_{-213}	4C26.42	double	two sided	Liuzzo et al. (2009a); White et al. (1997)
A2052	Y	94^{+84}_{-37}	3C317	bright core+halo (FRI)	two sided	Venturi et al. (2004); White et al. (1997)
A2152	Y	20^{+13}_{-20}	UGC10187	Tail rs	n.d.	White et al. (1997)
A2199	Y	97^{+9}_{-31}	3C338	double restarted	two sided	White et al. (1997); Feretti et al. (1993)
A2390	Y	247^{+43}_{-91}	B2151+174	MSO	two sided	Augusto et al. (2006); Allen et al. (2001)
A2597	Y	501^{+58}_{-512}	PKS 2322-123	asymmetric radiosource (FRI)	two sided	Taylor et al. (1999); Chen et al. (2007)

Mon. Not. R. Astron. Soc. **292**, 419–467 (1997)

An investigation of cooling flows and general cluster properties from an X-ray image deprojection analysis of 207 clusters of galaxies

D. A. White,[1]★ C. Jones[2] and W. Forman[2]

[1]*Institute of Astronomy, Madingley Road, Cambridge CB3 0HA*
[2]*Smithsonian Astrophysical Observatory, 60 Garden Street, Cambridge, MA 02138, USA*

Accepted 1997 August 6. Received 1997 July 15; in original form 1996 February 8

ABSTRACT

In this paper we present an X-ray image deprojection analysis of *Einstein Observatory* imaging data on 207 clusters of galaxies. The resulting radial profiles for luminosity, temperature and electron density variations are determined from the cluster surface-brightness profiles according to gravitational potential constraints from average X-ray temperatures and optical velocity dispersions. This enables us to determine cooling flow and other cluster properties, such as baryon fractions, Sunyaev–Zel'dovich microwave decrements and Thomson depths. From the results we have compiled a catalogue of the detected cooling flows, and investigated their effects on general cluster properties. To assist in the analysis, we have constructed self-consistent correlations between the cluster X-ray luminosity, temperature and optical velocity dispersion, using 'orthogonal distance' regression to account for errors in both dimensions of the data. These fits indicate that, in general, the temperatures of clusters are isothermal, and that they have spectral β-values consistent with unity (if the dependence of luminosity on temperature is assumed to be quadratic).

We find that the X-ray luminosity, temperature and optical velocity dispersion relations depend significantly on the cooling flow mass-deposition rate, through characteristic differences in the density profiles. Clusters of similar cooling flow mass-deposition rate exhibit self-similar density profiles, with larger cooling flows showing higher central densities. This leads to scatter in the luminosity-related correlations within the X-ray luminosity, temperature and optical velocity dispersion plane. The segregation in density also leads to dispersion in other related properties such as 'half-light radii' and baryon fractions. The baryon fraction in the cores of cooling flow clusters appears to be higher, but as the density profiles tend to a similar value at larger radii, irrespective of cooling flow property, so too do the baryon fraction profiles appear to rise to a concordant value of greater than 10 per cent at 1 Mpc. Thus this sample indicates that clusters, as a whole, are inconsistent with primordial nucleosynthesis baryon fraction prediction, for a flat universe, of 6 per cent.

Key words: catalogues – galaxies: clusters: general – cooling flows – galaxies: fundamental parameters – intergalactic medium – X-rays: galaxies.

1 INTRODUCTION

The technique of 'X-ray image deprojection' was first used in the study of the Cassiopeia A supernova remnant (Fabian et al. 1980), but its subsequent application to the Perseus cluster (Fabian et al. 1981) showed that it was particularly successful in the analysis of clusters of galaxies, especially those with cooling flows, because of their almost spherically symmetric appearance and highly peaked surface-brightness profiles. A benefit of the deprojection method (especially over detailed spectral analysis) is that it can easily be applied to fainter systems, allowing analysis for

★E-mail: daw@ast.cam.ac.uk

provided by TeV emission from blazars modeled as synchrotron photons generated in a mildly relativistic sheath inverse Compton scattered off electrons in a high Lorentz factor spine as indicated in Figure 22 (Ghisellini et al. 2005). However, alternatives such as rapid jet deceleration

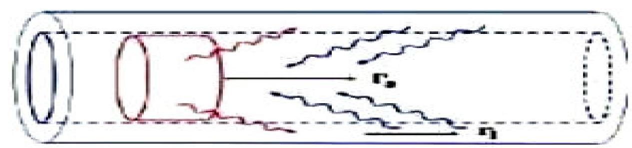

Figure 22. Inverse Compton scattered TeV photons (red) from a high Lorentz factor spine and initial photons (blue) from a mildly relativistic sheath.

(Georganopoulos, Perlman & Kazanas 2005; Kasznas & Georganopoulos 2006) can also generate TeV emission from photons emitted back towards the origin from the slowed jet that subsequently inverse Compton scatter off electrons in the higher Lorentz factor jet nearer to the origin.

6. Conclusion

What new things can we learn about AGN jets from astronomy at the highest angular resolution? We now have a reasonable theoretical scenario for the generation and collimation of jets. The scenario suggests a massive black hole surrounded by an accretion disk with jet spine and sheath generated by magnetic fields threading the ergosphere and accretion disk, respectively. The jet generation/launching region at $5 - 50R_S$, $0.5 - 5milli$pc, $5 - 50\mu$as is probably unresolved or only slightly resolved at the highest resolutions available. However, the initial acceleration/collimation region at $10 - 300R_S$, $1 - 100milli$pc, 10μas $- 1mas$ is resolvable at the highest resolutions available, and the transition region from Poynting flux dominated to kinetically dominated flow occurs at $\sim 300R_S$, ~ 0.1 pc, $\sim 1mas$ spatial and angular scales.

Tasks to be accomplished, roughly from larger to smaller scales and degree of difficulty:

(1) Locate the base of the kinetically dominated region. This is likely at the modified fast magnetosonic point and marks the outer limit to the transition region.

(2) Determine the jet flow/magnetic parameters and structure at the base of the kinetically dominated region.

(3) Determine the rate/shape of jet collimation out to the base of the kinetically dominated region.

(4) Determine the jet flow/magnetic parameters and structure in the magnetically dominated acceleration/collimation region.

(5) Link high energy emission, e.g., TeV emission, to shock structures (if produced in the kinetically dominated super-Alfvénic/magnetosonic flow region) or to magnetic reconnection structures (if produced in the magnetically dominated sub-Alfvénic flow region).

Accomplishing these tasks requires spatial and temporal motion, intensity/spectral and polarization observations at the smallest angular scales.

Suppose we use the image of the M87 jet base at $0.5mas$ resolution shown in Figure 23 (see also Walker in this proceedings) as a guide. With a black hole mass $\sim 3 \times 10^9$ solar masses and at a distance of ~ 17 Mpc, $R_S \sim 3\mu$as and the transition region $\sim 1mas$, the jet is likely largely kinetically dominated at the image angular scale but should show transverse and

2 THE MODEL

This section briefly summarizes the calculations presented in Reynolds et al. (1996) (following Marscher 1987) in order to demonstrate the method and define the parameters.

2.1 Limits on the magnetic field from SSA

With the assumption that the relativistic leptons have a distribution of Lorentz factors $N(\gamma) = N_0\gamma^{-p} = N_0\gamma^{-(2\alpha+1)}$, between $\gamma_{\rm min}$ and $\gamma_{\rm max}$, the spectrum in the optically thin regime is $S_\nu \propto \nu^{-\alpha}$. The corresponding relativistic lepton number density, n, is given by

$$n = \int_{\gamma_{\rm min}}^{\gamma_{\rm max}} N(\gamma)\mathrm{d}\gamma,$$

$$2\alpha n = -N_0\left[\gamma^{-2\alpha}\right]_{\gamma_{\rm min}}^{\gamma_{\rm max}}.$$

Therefore, for $\gamma_{\rm max} \gg \gamma_{\rm min}$ and $\alpha > 0.5$, the lepton number density is

$$n = \frac{N_0}{2\alpha}\gamma_{\rm min}^{-2\alpha}. \quad (1)$$

Initially we assume $\gamma_{\rm min} = 1$ for the following calculations. For a discussion of the effect of varying $\gamma_{\rm min}$ see Section 5.

The synchrotron flux in the optically thick (self-absorbed) region is independent of the particle density, resulting in an estimate on the magnetic field of

$$B \lesssim 10^{-5} b(\alpha)\theta_{\rm d}^4 \nu_{\rm m}^5 S_{\rm m}^{-2}\left(\frac{\delta}{1+z}\right)\mathrm{G}, \quad (2)$$

where the $\nu_{\rm m}$ and $S_{\rm m}$ are the frequency (in GHz) and flux density (in Jy) at spectral turnover. $\theta_{\rm d}$ is the angular diameter of the source in milliarcseconds (mas). As the angular diameter may be an upper limit (the core may not be fully resolved) this causes the estimate on B to be an upper limit. In some cases the source is elliptical, and in these cases the average $\theta_{\rm d} = \sqrt{\theta_{\rm a}\theta_{\rm b}}$, where $\theta_{\rm a}$ and $\theta_{\rm b}$ are the corresponding angular diameters of the ellipse. δ is the relativistic Doppler factor, defined as $\delta = 1/\Gamma(1 - \beta\cos\phi)$ where Γ and β are the Lorentz factor and v/c for the bulk motion of the jet, respectively, and ϕ is the angle between the line of sight and the jet axis. The function, $b(\alpha)$, is tabulated in Marscher (1987) and we have interpolated between the values given where appropriate.

The observation of compact radio sources with flat spectra, $\alpha_{\rm obs} \sim 0$, has been interpreted as the superposition of different SSA components each peaking at different frequencies (Blandford & Konigl 1979). Hence the observations at a given ν basically measure the flux density and the size of the component of the jet which is becoming self-absorbed at ν (in the observer's frame).

2.2 Limits on the magnetic field and number density

The jet becomes self-absorbed at an observed frequency, $\nu_{\rm m}$, where $\tau_{\rm syn}(\nu_{\rm m}, r) = \kappa(\nu_{\rm m})X = 1$; where $\kappa(\nu)$ is the synchrotron absorption coefficient, X is the path-length of the line of sight through the jet and r the jet cross-section radius. From Reynolds et al. (1996) and references therein

$$\kappa(\nu_{\rm m}) = \frac{3^{(\alpha+1)}\sqrt{\pi}g(\alpha)e^2 N_0}{8m_{\rm e}c}\nu_{\rm B}^{(3/2+\alpha)}\nu_{\rm m}^{-(5/2+\alpha)}\delta^{(5/2+\alpha)}, \quad (3)$$

where $\nu_{\rm B}$ is the cyclotron frequency and $g(\alpha)$ is the product of gamma functions (of the order of unity for the considered range of α).

This expression for $\kappa(\nu)$ is valid for $\nu \gg \nu_{\rm min} \sim \gamma_{\rm min}^2\nu_{\rm B}$, where $\nu_{\rm min}$ is the low-energy cut-off in the spectrum corresponding to the low-energy cut-off in the lepton energy distribution. In this case the self-absorption only depends on the normalization of the relativistic lepton distribution and the magnetic field.

The path-length is $X = 2r/\delta$, using the relativistic transformations for a cylindrical geometry. Combining this with equations (1) and (3), places a lower limit in the B–n plane for radiation at frequency $\nu_{\rm m}$ to be self-absorbed in the source,

$$nB^{(\frac{3}{2}+\alpha)} \gtrsim \frac{2\delta}{3^{(\alpha+1)}\sqrt{\pi}g(\alpha)\alpha\gamma_{\rm min}^{2\alpha}er}\left(\frac{m_{\rm e}c\nu_{\rm m}}{e\delta}\right)^{5/2+\alpha}. \quad (4)$$

2.3 Kinetic luminosity

The kinetic luminosity of the jet depends on the type of particles present, as well as their energy and number density. In the assumption that all of the energy contained within the jet results in the creation and expansion of the radio bubbles observed within clusters, then the power required to create these bubbles is an estimator of the (average) kinetic luminosity of the jet, that is, $L_{\rm K} = E_{\rm bubble}/t_{\rm bubble}$, where $t_{\rm bubble}$ is the creation time of the bubble. The simplest estimate on the energy required is that $E_{\rm bubble} = pV$, where V is the volume of the bubble, and p is the pressure of the surrounding intracluster gas. Taking into account any internal energy of the bubble results in

$$E_{\rm bubble} = \frac{\gamma_{\rm R}}{\gamma_{\rm R}-1}pV,$$

where $\gamma_{\rm R}$ is the ratio of specific heat capacities, which for a relativistic gas is 4/3, resulting in $E_{\rm bubble} = 4pV$. Whether the energy contained within the bubble is pV, $4pV$ or some other multiple of pV is currently uncertain. For example, investigating the weak shock surrounding the bubbles in the Perseus cluster, Fabian et al. (2006) find that the energy of the post-shock gas is around $2pV$. We use $E_{\rm bubble} = pV$, although using $4pV$ does not change the results significantly.

In our analysis we assume that the radio bubbles are in pressure equilibrium with their surroundings, whereas Reynolds et al. (1996) assumed that they were overpressured by a factor of ~3. Using their source parameters we recover the limits they place on the matter content of the M87 jet (see their fig. 1).

There are a number of estimates on the bubble time-scales. The most appropriate one for these young bubbles which are (presumably) still being inflated by their jet is the sound speed time-scale, $t_{\rm bubble} = 2R_{\rm bubble}/c_{\rm s}$, where $R_{\rm bubble}$ is the bubble radius and $c_{\rm s}$ is the local sound speed, following Dunn & Fabian (2004). There are no indications for strong shocks surrounding the bubbles, which implies that the bubble edges are travelling at less than the local sound speed. It is possible, however, that the bubbles do not grow smoothly, but in fits and starts (Fabian et al. 2005), and as such this time-scale is not a good estimate for the age of the bubble. For further discussion on time-scales relevant to the evolution of bubbles in clusters see Churazov et al. (2000), Dunn & Fabian (2004) and Dunn, Fabian & Taylor (2005).

As mentioned, we assume that the jet is particle dominated (i.e. we neglect the magnetic field contribution) and for simplicity, following other work (e.g. Sikora & Madejski 2000), assume that the protons are 'cold'. Thus the jet kinetic luminosity, including the advected energy, is

$$L_{\rm K} \approx \Gamma^2\beta\pi r\langle Z\rangle^2 nm_{\rm e}c^3\left[\frac{4}{3}(\langle\gamma\rangle - 1) + \frac{\Gamma-1}{\Gamma}(1+k_{\rm a})\right], \quad (5)$$

where $k_{\rm a}$ takes into account the effect of hadrons on the rest-mass energy (adapted from Schwartz et al. 2006). For electron–positron

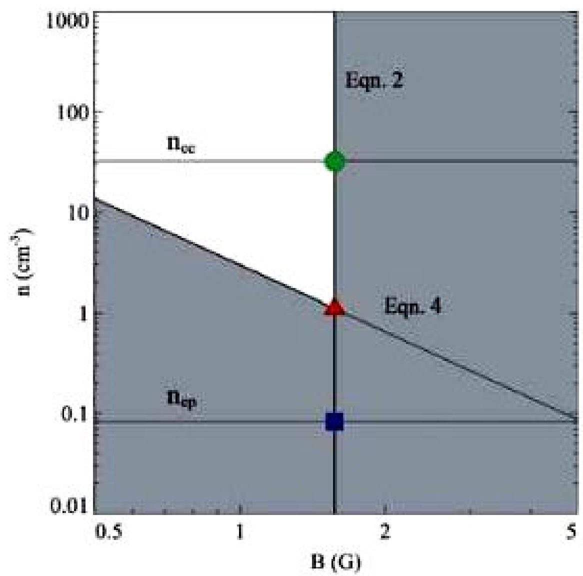

Figure 1. Constraints on the B–n plane from equations (2) and (4). The expected values for the number density for light and heavy jets from the estimated L_K are shown and correspond to the circle and square, respectively. The 'intersection point' (triangle) is the number density required from radio observations. This schematic corresponds to Kovalev-S_{Unres} from M87, and for clarity the uncertainties are not shown.